

1 Antibiotic darobactin mimics a β -strand to inhibit outer membrane
2 insertase
3
4
5

6 Hundeeep Kaur^{+,1}, Roman P. Jakob^{+,1}, Jan K. Marzinek², Robert Green³, Yu Imai³, Jani Reddy
7 Bolla⁴, Elia Agustoni¹, Carol V. Robinson^{4,5}, Peter J. Bond^{2,6}, Kim Lewis^{*,3}, Timm Maier^{*,1},
8 Sebastian Hiller^{*,1}
9

10
11 ¹Biozentrum, University of Basel, Switzerland

12 ²Bioinformatics Institute (A*STAR), 30 Biopolis Street, #07-01 Matrix, Singapore 138671,
13 Singapore

14 ³Antimicrobial Discovery Center, Department of Biology, Northeastern University, Boston
15 MA, USA

16 ⁴Physical and Theoretical Chemistry Laboratory, University of Oxford, South Parks Road,
17 Oxford OX1 3QZ, United Kingdom

18 ⁵The Kavli Institute for Nanoscience Discovery, Oxford, OX1 3QU

19 ⁶Department of Biological Sciences, National University of Singapore, 14 Science Drive 4,
20 Singapore 117543, Singapore.

21
22
23 ⁺ Equal contribution
24

25 * Correspondence: k.lewis@northeastern.edu; tim.maier@unibas.ch;
26 sebastian.hiller@unibas.ch
27
28
29

30 **Keywords:** membrane protein structure, antibiotics, outer membrane protein biogenesis, β -
31 strand augmentation, inhibition, cyclic peptides, molecular dynamics simulations, native mass
32 spectrometry, X-ray crystallography, cryo-electron microscopy

33 **Abstract**

34 **Antibiotics with novel modes of action targeting Gram-negative bacteria are needed to**
35 **resolve the antimicrobial resistance crisis¹⁻³. These pathogens are protected by an**
36 **additional outer membrane, rendering proteins on the cell surface attractive drug**
37 **targets^{4,5}. The natural compound darobactin targets the insertase BamA⁶, the central unit**
38 **of the essential BAM complex, which facilitates folding and insertion of outer membrane**
39 **proteins⁷⁻¹³. BamA lacks a typical catalytic center, and it is not obvious how a small**
40 **molecule such as darobactin might inhibit its function. Here, we resolve the darobactin**
41 **mode of action at the atomic level by a combination of cryo-electron microscopy, X-ray**
42 **crystallography, native mass spectrometry, *in vivo* experiments and molecular dynamics**
43 **simulations. Two unique cyclizations pre-organize the darobactin peptide in a rigid β -**
44 **strand conformation. This creates a mimic of the recognition signal of native substrates**
45 **with a superior ability to bind to the lateral gate of BamA. Upon binding, darobactin**
46 **replaces a lipid molecule from the lateral gate to use the membrane environment as an**
47 **extended binding pocket. Because the interaction between darobactin and BamA is**
48 **largely mediated by backbone contacts, it is particularly robust against potential**
49 **resistance mutations. Our results identify the lateral gate as a functional hotspot in BamA**
50 **and open the path for rational design of antibiotics targeting this bacterial Achilles heel.**

51 The BAM complex was purified from *E. coli* outer membranes (OMs), reconstituted in
52 n-dodecyl maltoside (DDM) micelles and incubated with darobactin A (darobactin). The cryo-
53 EM reconstruction at 3.0 Å resolution revealed the position of a bound darobactin molecule
54 (Fig. 1a, Extended Data Fig. 1, Supplementary Table 1). BamA features a lateral gate facing
55 the membrane, formed by strands β 1 and β 16 through a kink in strand β 16 at residue Gly807.
56 Previous work showed that substrate-free BamA exists in two interchanging conformations
57 with the gate either being open or being closed by the β 16-strand straightening to zip up against

58 $\beta 1^{14-16}$. Darobactin binds to the open form of the BamA lateral gate and essentially does not
59 perturb the structure of the BAM complex (Extended Data Fig. 2, Supplementary Table 2). To
60 better resolve the interaction, we crystallized the BamA β -barrel domain (BamA- β) with
61 darobactin in detergent micelles, and determined its structure at 2.3 Å resolution (Fig. 1b,
62 Supplementary Table 3). The position and bound conformation of darobactin in the cryo-EM
63 and crystal structures were essentially identical (Extended Data Fig. 2).

64 Darobactin A is a 965 Da heptapeptide with the linear sequence W¹-N²-W³-S⁴-K⁵-S⁶-
65 F⁷ that is cyclized twice. Darobactin binds to the BamA lateral gate in antiparallel β -sheet
66 conformation to the $\beta 1$ -strand via a series of backbone hydrogen bonds (Fig. 1c). These start
67 at Ile430 of BamA pairing to W¹ of darobactin and continue all the way to Gly424 paired to
68 F⁷. The C-terminal carboxyl group of darobactin contacts the side chain of Asn422, while the
69 N-terminus forms three backbone hydrogen bonds with Ile430 in strand $\beta 1$, Gly807 in $\beta 16$ and
70 Leu780 in turn 7. Additionally, the side chain of N² of darobactin forms a backbone hydrogen
71 bond with Lys808 and a side chain hydrogen bond with Asn427 in $\beta 1$ (Figs. 1c, 2a). The
72 observation that darobactin effectively seals the gate-open state of BamA was also confirmed
73 in aqueous solution by a comparison of 2D [¹⁵N, ¹H]-TROSY NMR spectra of BamA (Extended
74 Data Fig. 3)^{6,14,15}. Taken together, these data show that darobactin A is a molecular mimic of a
75 β -strand that seals the open lateral gate of BamA upon binding.

76 The dominance of backbone contacts in the interaction suggests that the binding affinity
77 will be only weakly sensitive to local changes in the BamA sequence. To test this hypothesis,
78 we carried out an alanine scan of the darobactin binding site (Asn422–Phe428 on strand $\beta 1$)
79 and determined for each mutant the affinity to darobactin by isothermal titration calorimetry
80 (ITC) (Fig. 2b, Extended Data Fig. 4, Supplementary Table 4). The affinity of darobactin to
81 wild type BamA- β was $K_D=0.6 \mu\text{M}$, in good agreement with previous measurements⁶.
82 Supporting our hypothesis, the alanine mutants T423A, G424A, S425A and F426A, which do

83 not feature side chain contacts with darobactin, show a K_D essentially identical to wild type.
84 The mutant N422A was also found to have wild-type affinity to darobactin, suggesting that its
85 side chain contact is not relevant for the interaction. Accordingly, none of these five mutations
86 had a clear effect on the functionality of BamA in a complementation assay in living cells
87 (Extended Data Fig. 3d). In contrast, residue Asn427 forms a relevant side chain interaction
88 with darobactin as evidenced by a 10-fold weaker binding to an N427A mutant. This *E. coli*
89 mutant, however, is not viable and therefore does not provide a way for bacteria to readily
90 acquire antibiotic resistance. These data show that darobactin is largely insensitive to amino
91 acid mutations in its binding site, which is unique for an antibiotic. Accordingly, darobactins
92 are variable in their amino acid composition⁶ and the amino acid sequence at the darobactin
93 binding site is not conserved among BamA homologues (Fig. 2c). Altogether, these findings
94 suggest a high robustness of the darobactin antibiotic efficacy against resistance mutations.

95 We further note that the binding pocket of darobactin is of a unique physico-chemical
96 nature, comprising a lipidic, a peptidic and an aqueous component. In the bound state, ~36%
97 of the darobactin surface is in contact with BamA, while ~26% is in contact with the lipid and
98 ~38% with the aqueous solution (Fig. 2d). The structures of darobactin in solution determined
99 by NMR spectroscopy⁶ and bound to BamA are perfectly overlapping for the first five residues
100 (Fig. 2e), demonstrating that the cyclizations render it a pre-ordered β -strand mimetic. In
101 agreement with this, the linear peptide WNWSKSF, for which only one of many conformations
102 will fit into this site, does not bind to BamA⁶. Furthermore, the tryptophan residues of
103 darobactin are positioned at the height of the aromatic head groups, in the region where
104 membrane proteins typically have aromatic girdles¹⁷⁻¹⁹. Overall, darobactin has thus evolved
105 to perfectly read out the conformation of the peptido-lipidic environment at the BamA lateral
106 gate.

107 To resolve the functional role of lipids interacting with the BamA–darobactin complex,
108 we performed explicitly solvated all-atom molecular dynamics (MD) simulations run in
109 triplicates of 1 μ s each of BamA- β in an *E. coli* OM-like asymmetric lipidic environment. In
110 the absence of darobactin, BamA- β adopted an open-gate conformation as the dominant state
111 (Fig. 3a,b, Extended Data Fig. 5). Strand β 16 was highly dynamic across all replicas, as
112 revealed by its time-dependent root mean square deviation (RMSD) with respect to the initial
113 structure. Cardiolipin (CL), 1-palmitoyl-2-oleoyl-sn-glycero-3-phosphoethanolamine (PE) or
114 1-palmitoyl-2-oleoyl-sn-glycero-3-phosphoglycerol (PG) lipid molecules spontaneously
115 entered the lateral gate region, forming direct contacts between their acyl tails and residues
116 Ile430 and Leu780. The presence of lipid or detergent molecules in the gate has also been
117 observed in crystal structures of BamA- β stabilized by nanobodies¹⁴ and its homolog TamA²⁰.
118 Additionally, interaction of lipopolysaccharide (LPS) lipid head groups with the extracellular
119 loop L6 of BamA was observed in the simulations (Fig. 3b). The loop appears to drag one or
120 two neighboring LPS molecules deeper into the bilayer, and this might represent a lower energy
121 pathway for permeation of darobactin along the BamA surface to its target site.

122 The MD simulations of the BamA–darobactin complex exhibited a very stable
123 conformation, as indicated by the RMSD of strand β 16 (Extended Data Fig. 5). A total of 16
124 residues of BamA formed contacts with darobactin (Arg421, Thr423–Ile430, Val444, Leu780,
125 Gly781 and Gly807–Trp810, Extended Data Fig. 5b) out of which six residues (Phe426–
126 Ile430, Leu780) maintained the interactions throughout the entire simulation time across all
127 replicas. This implies that the lipid interaction mediated by Ile430 and Leu780 is replaced by
128 the tighter interaction with darobactin (Fig. 3c). Darobactin binding significantly decreased the
129 density of lipid phosphates at the dynamic gate region and loop-L6 in BamA- β . Additionally,
130 the K⁵ side chain of bound darobactin, which points away from BamA (Fig. 3d), interacted
131 primarily with the negatively charged phosphate moieties of PG and CL lipids.

132 We then used native mass spectrometry to validate the interplay of lipid and darobactin
133 interactions on the intact BAM complex. In three separate experiments we incubated 3 μ M of
134 the BAM complex with 5 μ M of one of the lipids PE, PG, or CL and recorded native mass
135 spectra (Extended Data Fig. 6). Lipid adduct peaks were observed for the entire BAM complex
136 and its subcomplexes. Notably, the negatively charged lipids PG and CL apparently have a
137 higher affinity, confirming the results from the MD simulations and previous observations that
138 the BAM complex analyzed from native membranes has CL-bound peaks²¹. We then incubated
139 these BAM:lipid complexes with 1 μ M darobactin. Darobactin binds both to lipid-bound and
140 lipid-free species of BAM. This is in perfect agreement with the observation from the MD
141 simulations that a ternary complex of BAM, darobactin and CL forms, and that darobactin
142 binding to the BAM:CL complex is significantly higher than for BAM:PG or BAM:PE (Fig.
143 3e). To determine the selectivity for specific lipids, we incubated BAM–darobactin with
144 mixtures of PE + CL or PG + CL. In both cases, darobactin significantly enriched on CL-bound
145 species, with an additional increase observed for 2xCL bound species. Taken together, the
146 combination of MD simulations and native mass spectrometry shows that CL binds as a
147 preferred lipid to both the ligand-free and the darobactin-bound BAM complex and enhances
148 the interaction of BamA with darobactin.

149 We next sought to elucidate the mode of resistance of three darobactin-resistant mutants
150 that were previously identified⁶, by *in silico* mutations within MD simulations and by *in vitro*
151 affinity measurements. Each of the mutants contains a double or a triple mutation (Fig. 4a,
152 Extended Data Fig. 7, Supplementary Table 5). In MD simulations of strain 1, the bulky side
153 chain addition G429V disrupted the interactions between the darobactin N² side chain and
154 Lys808, followed by loss of contacts between the BamA C-terminal region of strand β -16 and
155 darobactin (Extended Data Fig. 7a). The single mutation G807V, in turn, led to a 100-fold
156 decreased affinity for darobactin. Correspondingly, each of the single point mutations

157 increased the MIC by 16-fold and their combination by more than 32-fold. In strain 2, the
158 E435K mutation induced an allosteric effect by interacting with the neighboring acidic residues
159 Asp498 and Asp500, destabilizing hairpin $\beta 1/\beta 2$ and leading to a $\sim 20\%$ decrease in darobactin
160 contacts compared to wild type (Extended Data Fig. 7b). Accordingly, these mutations
161 increased the MIC by more than 32-fold. For strain 3, the single mutation Q445P led to a kink
162 in strand $\beta 2$, which resulted in a highly dynamic hairpin $\beta 1/\beta 2$, leading to a loosening of the
163 interaction with darobactin *in silico* and a complete loss of the affinity *in vitro* (Extended Data
164 Fig. 7c). The same mutation increased the *in vivo* MIC 2-fold, and the additional mutation
165 T434A mutation led to another eight-fold increase in MIC. Importantly, while all of these
166 mutations confer resistance to darobactin in rich medium, all of them come at the cost of
167 compromising *E. coli* virulence⁶.

168 Notably, the data obtained so far does not allow to distinguish whether darobactin kills
169 its target bacteria by acting as an inhibitor of BamA, or by creating a toxic entity in complex
170 with BamA. To distinguish between the two possibilities, we performed experiments with
171 diploid strains carrying both wild-type BamA and a resistant mutant protein (Supplementary
172 Table 6). In several different combinations, the resulting MICs corresponded in each case to
173 those of the resistant strain and not to the lower wild-type MIC, clearly ruling out the scenario
174 of a toxic entity, and demonstrating that darobactin acts as an inhibitor of BamA function.

175 An important feature of darobactin towards its practical application is its inactivity
176 against gut symbionts including the Gram-negative *Bacteroides*^{6,22}. We wondered whether
177 their resistance might be explained by the composition of the darobactin interaction site
178 (Extended Data Fig. 8). The amino acid sequence comparison of BamA from different species
179 indicates that the Gly424 of $\beta 1$ -strand in *E. coli* is conserved in all Gram-negatives except for
180 *Bacteroides*. The single point mutant G424D, which locally converts the *E. coli* sequence to
181 *Bacteriodes*, showed a slightly reduced *in vitro* affinity to darobactin compared to wild type

182 (Fig. 2b). We then tested chimeric strains where the binding-site sequence of strand β 1
183 (GSFNFG in *E. coli*) was replaced with either that of *Acinetobacter baumannii* (GTTTLA) or
184 *Bacteroides fragilis* (DQVEFS). But even with such drastic changes in the sequence of β 1-
185 strand, the *in vitro* affinity to darobactin changed only around 10-fold, similar to the single
186 point mutation N427A, and accordingly, the associated change in MIC was increased by only
187 2- or 4-fold for *E. coli* with *Bacteroides* or *A. baumannii* sequences, respectively
188 (Supplementary Table 5). These data indicate that the insensitivity of *Bacteroides* to darobactin
189 cannot be explained solely by the primary sequence of strand β 1, but that other factors must
190 also contribute, such as the sequence differences in other regions, a different permeability of
191 the outer membrane, the involvement of other molecules, or a reduced essentiality of the
192 targeted BAM in *Bacteroides*. Similar considerations hold for the so far unexplained resistance
193 of the darobactin producer strain.

194 The physiological role of the BAM complex is to fold β -barrel outer membrane proteins
195 (OMPs) into the OM^{23,24}. Most BAM substrates contain a consensus signal sequence at their
196 C-terminus including a conserved terminal aromatic residue^{25,26}. The first step of the insertase-
197 activity mediated by BamA likely involves anchoring of this signal sequence to the lateral gate
198 region, as evidenced by chemical cross-linking^{8,27}, and structurally trapped folding
199 intermediates^{28,29}. In a recently reported structure of a late-stage intermediate²⁹, a substrate
200 BamA binds with its C-terminal strand β 16 to strand β 1 in such a way that the C-terminal
201 aromatic residue W810 ends up in the same position where the C-terminal Phe of darobactin
202 binds (Fig. 4b, Extended Data Fig. 9a–f). Darobactin resembles typical β -signal sequences both
203 by its alternating hydrophobicity and by the presence of a C-terminal phenylalanine. Albeit not
204 being the most prototypic β -signal, the darobactin sequence is within the peptide space spanned
205 by all known β -signals (Extended Data Figure 9 g–j).

206 Together, the data suggest that darobactin blocks the first step of the insertion reaction
207 catalyzed by BamA (Fig. 4c). While the β -signal sequences of substrates have evolved to attach
208 only transiently to the gate region of BamA, darobactin's preformed β -strand binds with high
209 affinity, presumably locally outcompeting all cognate substrates. We tested this model in
210 competition binding experiments between darobactin and β -signal peptides from four different
211 OMPs, as well as a β -signal consensus sequence. Each of the five peptides interacted only
212 weakly with BamA- β , with dissociation constants at least three orders of magnitude higher
213 than for darobactin (Extended Data Figure 10, Supplementary Table 7). Even if the total
214 affinity of OMP substrates to BAM *in situ* is enhanced by additional interactions, this huge
215 affinity difference represents strong evidence that darobactin will locally outcompete β -signal
216 peptides also in the native context.

217 Altogether, our findings highlight the lateral gate as a key target site for antibiotics and
218 darobactin as a promising lead compound. The structure of the BAM-darobactin complex also
219 adds information for understanding other reported BamA inhibitors^{6,30-32} and provides a path
220 forward for *de novo* design and optimization of compounds to target an essential surface protein
221 of Gram-negative pathogens.

222

223 **References**

- 224 1 Brown, E. D. & Wright, G. D. Antibacterial drug discovery in the resistance era. *Nature*
225 **529**, 336-343, (2016).
- 226 2 Lewis, K. The science of antibiotic discovery. *Cell* **181**, 29-45, (2020).
- 227 3 Tacconelli, E. *et al.* Discovery, research, and development of new antibiotics: the WHO
228 priority list of antibiotic-resistant bacteria and tuberculosis. *Lancet Infect Dis* **18**, 318-
229 327, (2018).
- 230 4 Epanand, R. M., Walker, C., Epanand, R. F. & Magarvey, N. A. Molecular mechanisms of
231 membrane targeting antibiotics. *Biochim Biophys Acta* **1858**, 980-987, (2016).
- 232 5 Srinivas, N. *et al.* Peptidomimetic antibiotics target outer-membrane biogenesis in
233 *Pseudomonas aeruginosa*. *Science* **327**, 1010-1013, (2010).
- 234 6 Imai, Y. *et al.* A new antibiotic selectively kills Gram-negative pathogens. *Nature* **576**,
235 459-464, (2019).
- 236 7 Bakelar, J., Buchanan, S. K. & Noinaj, N. The structure of the β -barrel assembly
237 machinery complex. *Science* **351**, 180-186, (2016).
- 238 8 Doyle, M. T. & Bernstein, H. D. Bacterial outer membrane proteins assemble via
239 asymmetric interactions with the BamA β -barrel. *Nat Commun* **10**, 3358, (2019).
- 240 9 Gu, Y. *et al.* Structural basis of outer membrane protein insertion by the BAM complex.
241 *Nature* **531**, 64-69, (2016).
- 242 10 Iadanza, M. G. *et al.* Lateral opening in the intact β -barrel assembly machinery captured
243 by cryo-EM. *Nat Commun* **7**, 12865, (2016).
- 244 11 Konovalova, A., Kahne, D. E. & Silhavy, T. J. Outer membrane biogenesis. *Annu Rev*
245 *Microbiol* **71**, 539-556, (2017).
- 246 12 Lee, J. *et al.* Formation of a beta-barrel membrane protein is catalyzed by the interior
247 surface of the assembly machine protein BamA. *Elife* **8**, (2019).
- 248 13 Noinaj, N. *et al.* Structural insight into the biogenesis of β -barrel membrane proteins.
249 *Nature* **501**, 385-390, (2013).
- 250 14 Kaur, H. *et al.* Identification of conformation-selective nanobodies against the
251 membrane protein insertase BamA by an integrated structural biology approach. *J*
252 *Biomol NMR*, (2019).
- 253 15 Hartmann, J. B., Zahn, M., Burmann, I. M., Bibow, S. & Hiller, S. Sequence-specific
254 solution NMR assignments of the β -barrel insertase BamA to monitor its
255 conformational ensemble at the atomic level. *J Am Chem Soc* **140**, 11252-11260,
256 (2018).
- 257 16 Ni, D. *et al.* Structural and functional analysis of the β -barrel domain of BamA from
258 *Escherichia coli*. *FASEB J* **28**, 2677-2685, (2014).
- 259 17 Hong, H., Park, S., Jimenez, R. H., Rinehart, D. & Tamm, L. K. Role of aromatic side
260 chains in the folding and thermodynamic stability of integral membrane proteins. *J Am*
261 *Chem Soc* **129**, 8320-8327, (2007).
- 262 18 Lee, A. G. Lipid-protein interactions in biological membranes: a structural perspective.
263 *Biochim Biophys Acta* **1612**, 1-40, (2003).
- 264 19 Schulz, G. E. The structure of bacterial outer membrane proteins. *Biochim Biophys Acta*
265 **1565**, 308-317, (2002).
- 266 20 Gruss, F. *et al.* The structural basis of autotransporter translocation by TamA. *Nat*
267 *Struct Mol Biol* **20**, 1318-1320, (2013).
- 268 21 Chorev, D. S. *et al.* Protein assemblies ejected directly from native membranes yield
269 complexes for mass spectrometry. *Science* **362**, 829-834, (2018).
- 270 22 Wexler, H. M. Bacteroides: the good, the bad, and the nitty-gritty. *Clin Microbiol Rev*
271 **20**, 593-621, (2007).

272 23 Knowles, T. J., Scott-Tucker, A., Overduin, M. & Henderson, I. R. Membrane protein
273 architects: the role of the BAM complex in outer membrane protein assembly. *Nat Rev*
274 *Microbiol* **7**, 206-214, (2009).

275 24 Noinaj, N., Rollauer, S. E. & Buchanan, S. K. The β -barrel membrane protein insertase
276 machinery from Gram-negative bacteria. *Curr Opin Struct Biol* **31**, 35-42, (2015).

277 25 Robert, V. *et al.* Assembly factor Omp85 recognizes its outer membrane protein
278 substrates by a species-specific C-terminal motif. *PLoS Biol* **4**, e377, (2006).

279 26 Stubenrauch, C. *et al.* Effective assembly of fimbriae in *Escherichia coli* depends on
280 the translocation assembly module nanomachine. *Nat Microbiol* **1**, 16064, (2016).

281 27 Hohr, A. I. C. *et al.* Membrane protein insertion through a mitochondrial β -barrel gate.
282 *Science* **359**, (2018).

283 28 Xiao, L. *et al.* Structures of the β -barrel assembly machine recognizing outer membrane
284 protein substrates. *The FASEB Journal* **35**, e21207, (2021).

285 29 Tomasek, D. *et al.* Structure of a nascent membrane protein as it folds on the BAM
286 complex. *Nature* **583**, 473-478, (2020).

287 30 Hart, E. M. *et al.* A small-molecule inhibitor of BamA impervious to efflux and the
288 outer membrane permeability barrier. *Proc Natl Acad Sci USA* **116**, 21748-21757,
289 (2019).

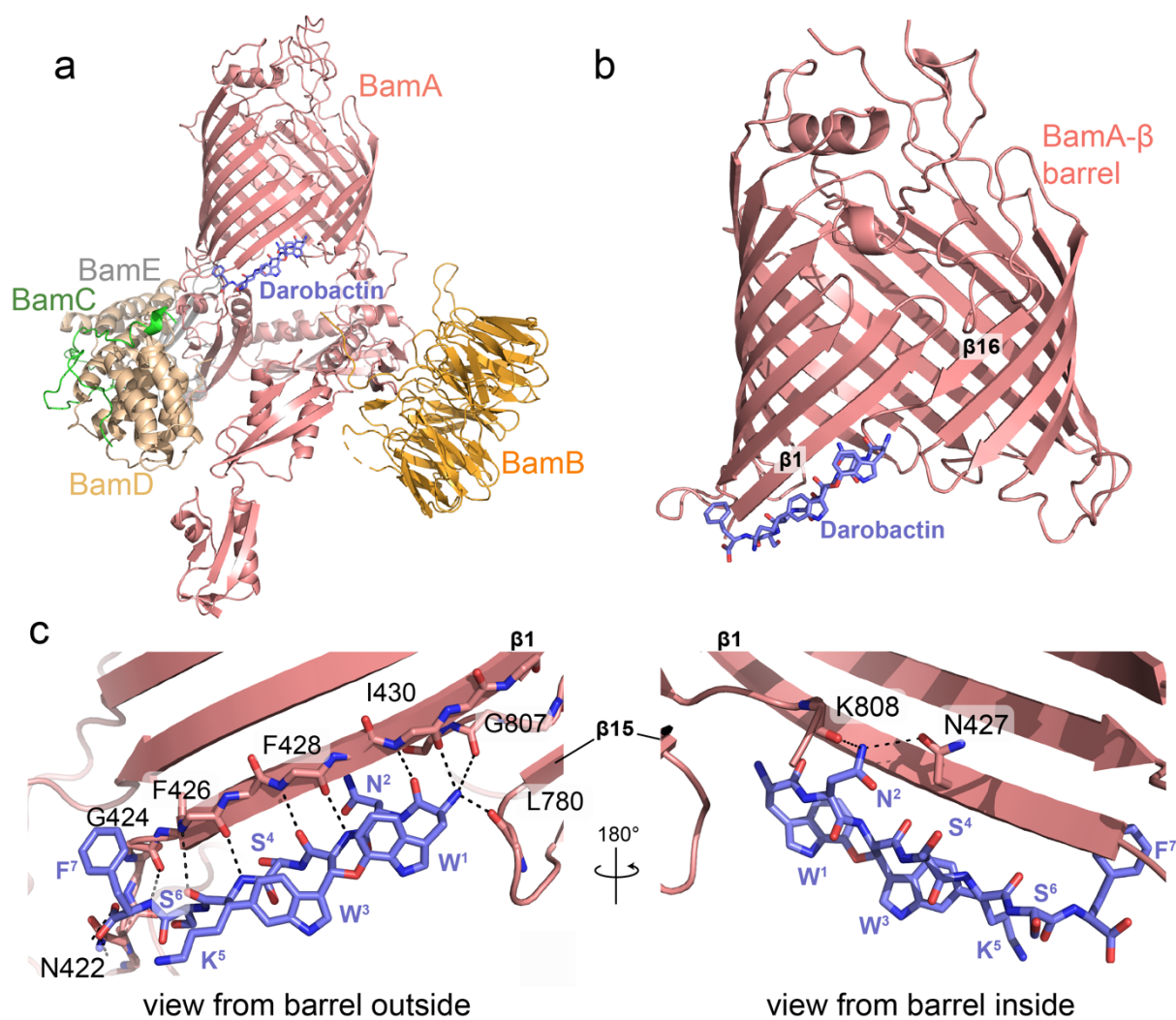
290 31 Luther, A. *et al.* Chimeric peptidomimetic antibiotics against Gram-negative bacteria.
291 *Nature* **576**, 452-458, (2019).

292 32 Storek, K. M. *et al.* Monoclonal antibody targeting the β -barrel assembly machine of
293 *Escherichia coli* is bactericidal. *Proc Natl Acad Sci USA* **115**, 3692-3697, (2018).

294

295 **Figures**

296



297

298 **Figure 1. Structural basis of darobactin function.** (a) Three-dimensional structure of the

299 BAM complex in DDM micelles with bound darobactin, resolved by cryo-EM to a resolution

300 of 3.0 Å. The five proteins BamA–BamE are shown in cartoon mode with colors as annotated.

301 Darobactin (blue) is shown in stick representation. (b) Crystal structure of the BamA β -barrel

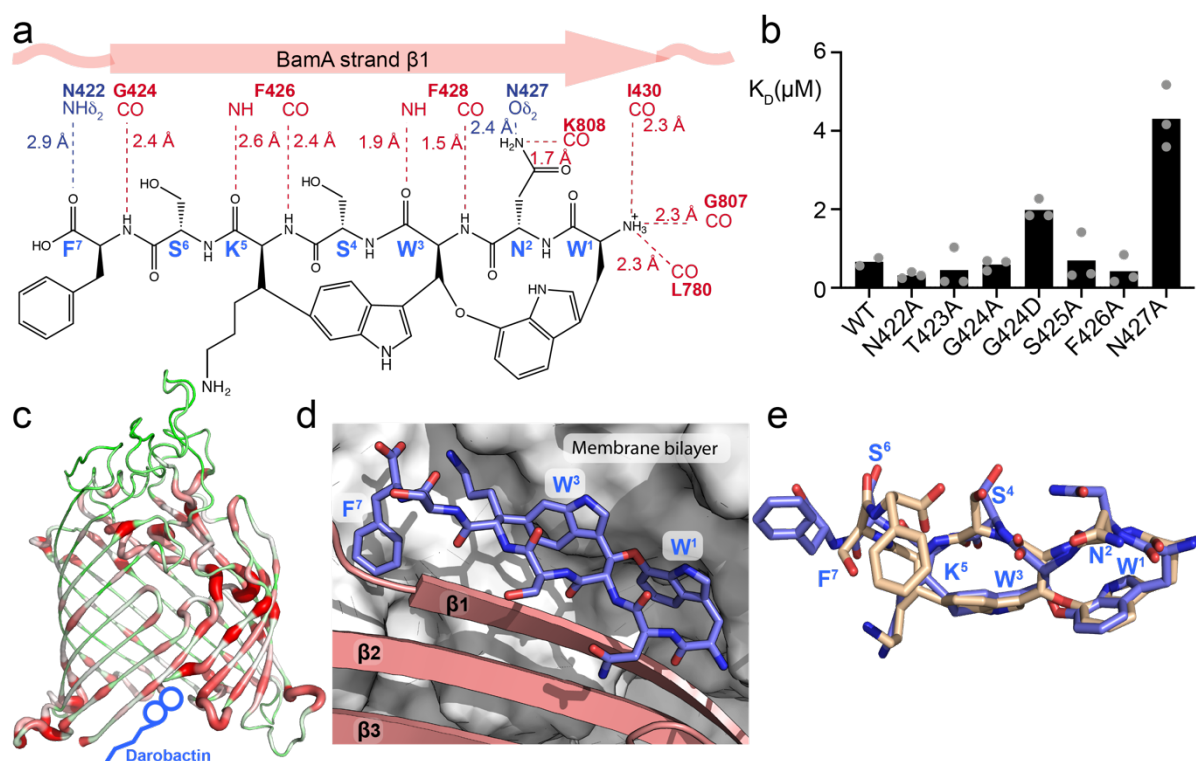
302 in detergent micelles with bound darobactin, resolved to 2.3 Å resolution. Colors as in a. (c)

303 Detailed view of the BamA–darobactin interaction site. Amino acid residues involved in

304 binding are shown in stick representation and direct contacts are shown as dashed lines.

305 Darobactin residues are labeled W¹N²W³S⁴K⁵S⁶F⁷.

306



308

309

310 **Figure 2. The unique proteo-lipidic binding pocket of darobactin.** (a) Map of the hydrogen

311 bonds between darobactin and BamA. Canonical β -strand hydrogen-bonds and side chain

312 interactions are shown by red and blue lines, respectively. (b) Affinity of darobactin for

313 different BamA β -barrel variants in LDAO micelles as determined by ITC. Individual

314 measurements are shown as grey dots and the resulting average as a black bar. $n=3$ independent

315 experiments per condition, $n=2$ for wild type. (c) BamA β -barrel in sausage representation,

316 with sequence conservation ranging from low (thin, green) to high (thick, red). The binding

317 site of darobactin is indicated. (d) Three-dimensional visualization of the darobactin binding

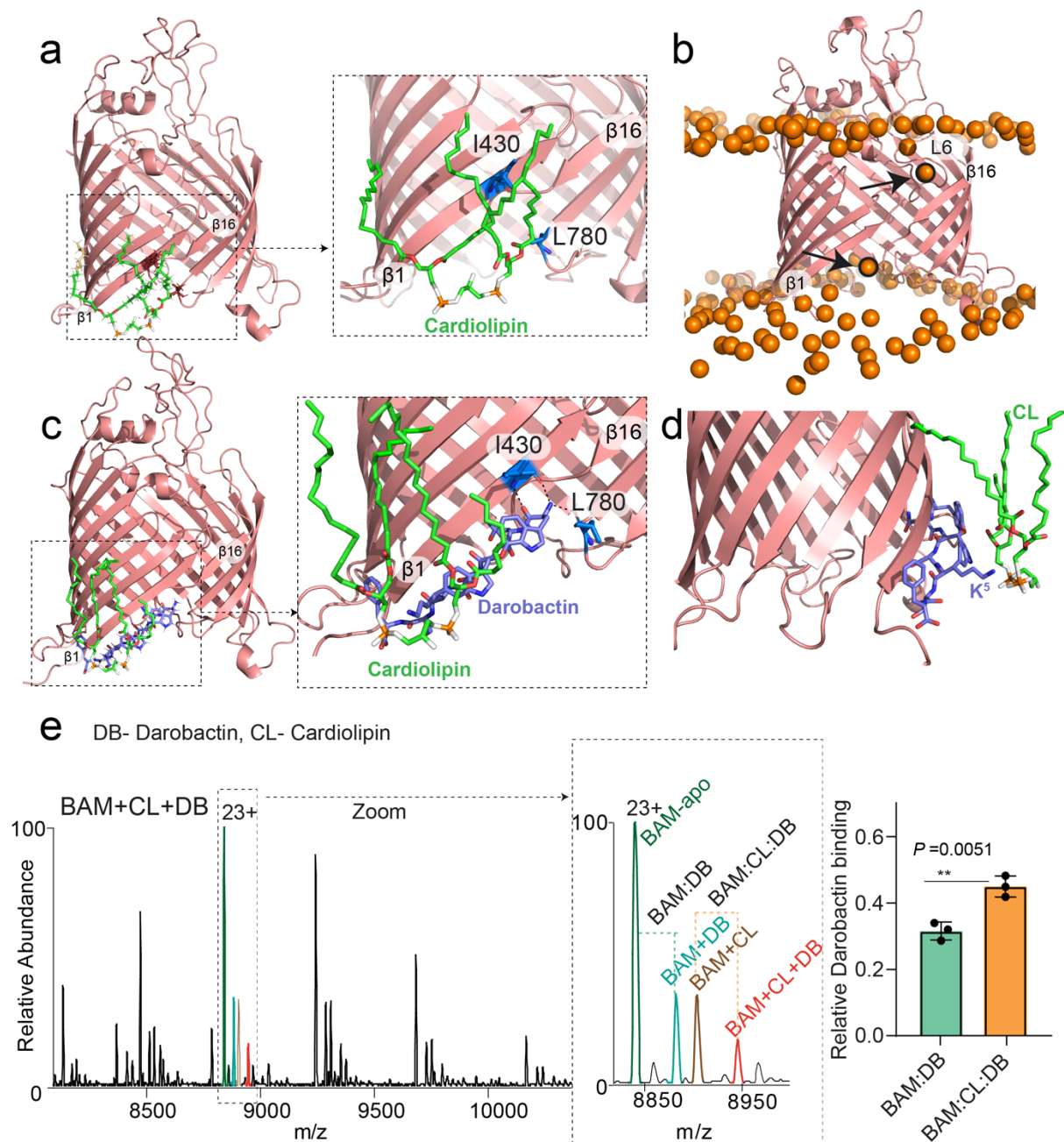
318 pocket formed by lipids, protein and water, obtained by extracting the most dominant

319 conformation from MD simulations. (e) Superposition of the structures of free darobactin in

320 solution as determined by NMR spectroscopy (beige) and darobactin in its conformation bound

321 to BamA (blue).

322



323

324 **Figure 3. Lipid dynamics of BamA–darobactin in the *E. coli* membrane.** (a, b)

325 Representative snapshots from MD simulations of the darobactin-free state, illustrating: (a) a

326 CL molecule anchored to the gate region by Ile430 and Leu780; (b) the interaction of lipid

327 phosphates (orange spheres) with BamA. Two lipid molecules translocated from their

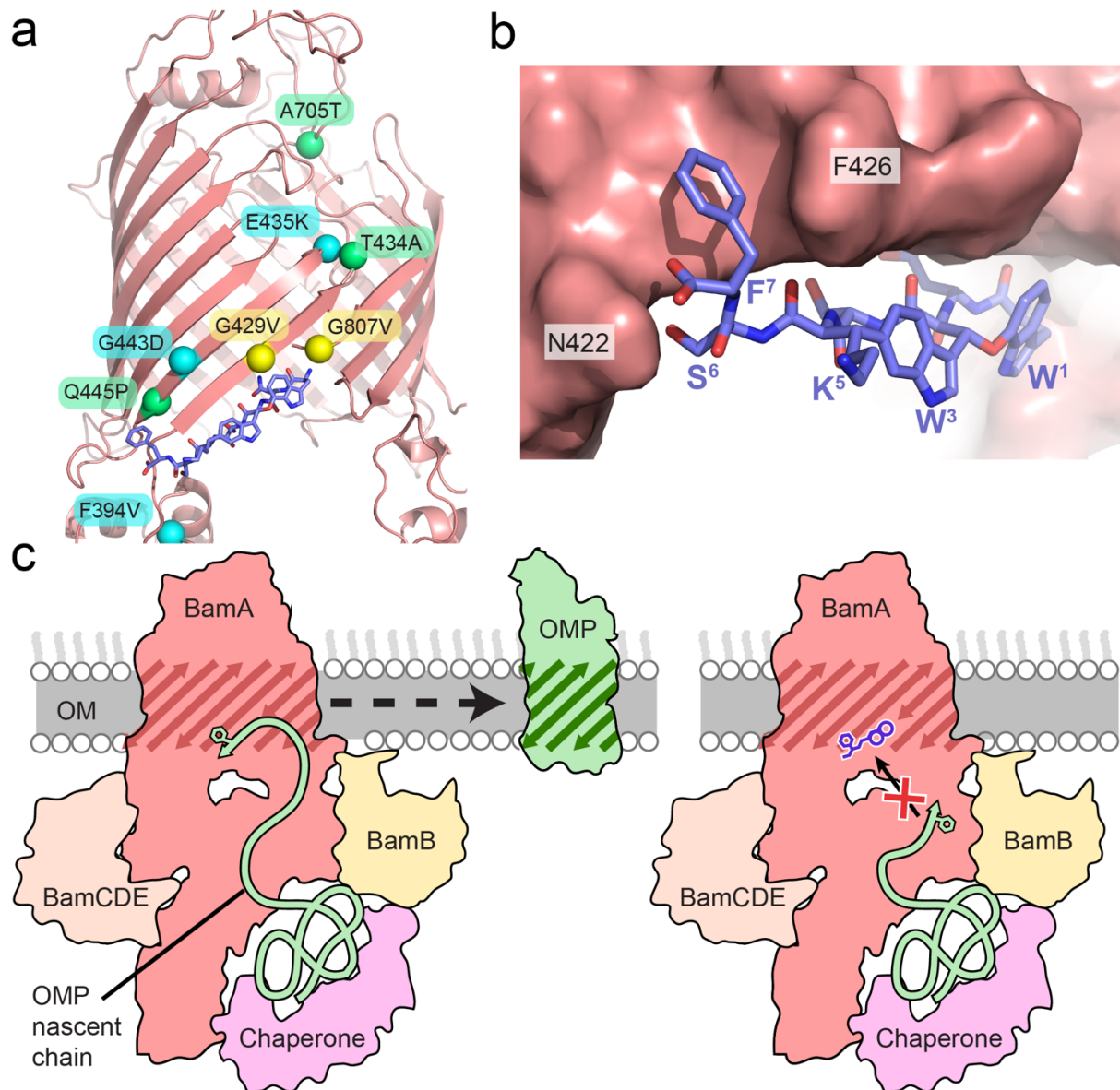
328 canonical positions are highlighted with arrows. (c, d) Representative snapshots from MD

329 simulations of the BamA-darobactin complex, illustrating: (c) darobactin bound tightly to the

330 gate region interacting with Ile430 and Leu780. (d) K⁵ of darobactin interacting with the

331 negatively charged CL headgroup. (e) Mass spectra of BAM complex with CL and darobactin.
332 CL, darobactin and their combination adduct peaks are highlighted in the zoom-in section of
333 the charge state 23+. Bar chart of relative darobactin bound peak intensities indicate that
334 darobactin co-bound with CL is observed to a greater extent than bound alone. Bars represent
335 mean \pm s.d., points show data from three independent experiments, $**P=0.0051$. $*P < 0.05$;
336 $**P < 0.01$; two-tailed unpaired Student's t-test.

337



338
339

340 **Figure 4. Mechanism of darobactin action.** (a) Location of amino acid mutations from three
 341 darobactin-resistant strains 1, 2 and 3 shown on the BamA–darobactin structure in yellow, cyan
 342 and green, respectively. (b) Surface view of BamA- β highlighting the binding site of darobactin
 343 F⁷. (c) In its native function, BamA recognizes the consensus β -signal in OMP nascent chains
 344 and folds and inserts them into the membrane (left panel). Darobactin binds to the dynamic
 345 lateral gate of BamA, blocking the β -signal binding site and thus BamA function (right panel).

346

347 **Online Methods**

348

349 **Protein expression and purification**

350 The barrel domain of BamA, here referred to as BamA- β , (residues 421–810, C690S, C700S)
351 with a C-terminal hexa-His-tag was overexpressed and purified as described previously^{14,33}.
352 Briefly, the protein was overexpressed in inclusion bodies using BL21(DE3) containing the
353 Lemo System. The cells were resuspended in the lysis buffer (50 mM Tris-HCl, 300 mM NaCl,
354 pH 8.0) and lysed by sonication to obtain BamA- β containing inclusion bodies. The inclusion
355 bodies were solubilized in 50 mM Tris-HCl, 300 mM NaCl, 2 (pH 8.0), buffer with 6 M
356 Guanidine-HCl and unfolded BamA- β was purified using Ni-NTA chromatography. The
357 purified protein was precipitated overnight by dialyzing against ultrapure H₂O. The precipitates
358 were pelleted by centrifugation at 30,000 g and resolubilized in the 6M Guanidinium
359 hydrochloride buffer. This highly concentrated and pure unfolded BamA- β was refolded by
360 adding it dropwise in buffer with 0.5% w/v LDAO micelles (50 mM Tris-HCl, 300 mM NaCl,
361 500 mM Arginine, 0.5% w/v LDAO, pH 8.0). The refolded protein was dialysed against 50
362 mM Tris, pH 8.0 overnight. Properly folded protein was further obtained using anion ion
363 exchange chromatography using a linear gradient starting from no NaCl to 0.5 M NaCl.
364 Correctly folded protein peak was collected and concentrated to exchange it into the desired
365 buffer using size exclusion chromatography. For crystallization, the protein was expressed in
366 Luria Broth (LB) and purified using the above-mentioned protocol. The buffer composition for
367 size exclusion chromatography (SEC) prior to crystallization was 20 mM Tris pH 7.5, 150 mM
368 NaCl, 0.05% w/v LDAO and 0.35% w/v C₈E₄. The same protocol was used for all the BamA-
369 β barrel mutants.

370 For the expression of the BAM complex, one plasmid containing all five *E. coli* BamA–E genes
371 was chemically synthesized (GenScript), in which BamE was C-terminally linked to a His₆-tag
372 and BamB C-terminally linked to a StrepII-tag. The BAM complex was expressed in *E. coli*

373 BL21(DE3) C43 cells in LB medium in the presence of 100 $\mu\text{g}/\text{mL}$ ampicillin. Cells were
374 grown at 37°C until an OD_{600} of 0.6, then induced with 0.1 mM isopropyl- β -D-1-
375 thiogalactopyranoside (IPTG) and further cultivated over night at 20°C. Cells were
376 resuspended in ice cold Tris-buffered saline (TBS; 50 mM Tris pH 8.0, 300 mM NaCl)
377 homogenized with a douncer, lysed using a microfluidizer and pelleted by ultracentrifugation
378 with a 45 Ti rotor (220,000 g, 2h, 4°C). The BAM complex was extracted from the pellet with
379 TBS containing 3% (v/v) Eluent (Calbiochem). After ultracentrifugation with a 45 Ti rotor
380 (220,000 g, 30 min, 4°C), the supernatant was loaded on a Ni Sepharose FF column, washed
381 with 20CV of TBS containing 0.05% DDM and eluted with TBS containing 0.05% (w/v) DDM
382 and 500 mM imidazole. The eluate was directly loaded on a Strep-Tactin XT column (IBA)
383 and eluted with TBS containing 0.05% DDM and 10 mM biotin. Finally, the BAM complex
384 protein was purified on a 16/600 Superdex 200 column (GE Healthcare) using 20 mM Tris pH
385 8.0, 150 mM NaCl, 0.05% (w/v) n-dodecyl β -D-maltopyranoside (DDM) and concentrated to
386 5–10 mg/ml and directly flash frozen in liquid nitrogen.

387

388 **Crystallization, X-ray data collection and structure determination**

389 The BamA- β -darobactin complex was assembled by mixing BamA- β (10 mg/ml) with a 1.5-
390 fold molar excess of darobactin. All crystallization experiments were carried out in sitting-drop
391 vapor diffusion experiments at room temperature mixing equal volumes of protein and
392 reservoir solution. Rod-like crystals (space group I2, $a=69.99$, $b=82.56$, $c=94.30$, $\alpha=90^\circ$,
393 $\beta=108.64^\circ$, $\gamma=90^\circ$) were grown in 0.06 M Magnesium chloride/Calcium Chloride, 0.1 M
394 imidazole/2-(N-morpholino)ethanesulfonic acid pH 6.5, 12.5% v/v 2-Methyl-2,4-pentanediol,
395 12.5% w/v Polyethylene glycol 1,000, and 12.5% w/v Polyethylene glycol 3,350 and directly
396 flash frozen in liquid nitrogen. Rhomboid crystals (space group I2, $a=79.61$, $b=79.81$, $c=89.34$,
397 $\alpha=90^\circ$, $\beta=106.42^\circ$, $\gamma=90^\circ$) were grown slowly over several weeks in 0.1 M Magnesium

398 chloride, 0.03 M Tris pH 8.0, 19% w/v Polyethylene glycol 4,000 and were cryopreserved by
399 the addition of 20% ethylene glycol (v/v) and flash-cooled with liquid nitrogen. All data were
400 collected at the SLS beamline X06SA (Swiss Light Source, Paul Scherrer Institute,
401 Switzerland) at 100 K. Data were integrated, indexed with XDS³⁴ and scaled using aimless³⁵.
402 The structures were solved by molecular replacement using the crystal structure of
403 6QGW.pdb¹⁴ as search model with the program PHASER³⁶. Model building was performed
404 with Coot³⁷, ligand restraints are derived from PRODRG³⁸ and the structures were refined with
405 PHENIX³⁹. MolProbity⁴⁰ was used to evaluate the finale model and PyMOL⁴¹ for protein
406 model visualization. Data and Refinement statistics are summarized in Supplementary Table
407 3.

408

409 **Electron microscopy sample preparation and data collection**

410 A 4 μ l aliquot of BAM complex in 20 mM Tris pH 8.0, 150 mM NaCl, 0.05% (w/v) n-dodecyl
411 β -D-maltopyranoside (DDM) at a concentration of 5.5 mg/ml with a 2-fold molar excess of
412 darobactin was applied to a C-Flat CF-1.2/1.3-2C (Electron Microscopy Sciences) allowed to
413 incubate at room temperature and 100% humidity for 30 s, then manually blotted with a
414 Whatman filter paper. A second 4 μ l aliquot of BAM solution was added, and the grid blotted
415 and vitrified by plunging into liquid ethane using a Vitrobot (FEI, Vitrobot III). Grid quality
416 was analyzed using a Glacios Cryo-TEM cryo-transmission electron microscope, operated at
417 an acceleration voltage of 200 kV. Final data was collected using a Titan Krios electron
418 microscope (FEI) operated at 300 kV, a GIF Quantum LS imaging filter (Gatan) and a K2
419 Summit (Gatan) operating in counting mode using SerialEM⁴². Images were acquired at 0.8–
420 2.0 μ m defocus and a nominal magnification of 165,000 \times , corresponding to a pixel size of
421 0.82 \AA (Supplementary Table 1). Movies were collected with a total dose of approximately 50
422 $e^-/\text{\AA}^2$ per 9 s exposure, fractionated over 45 frames, using beam-image shift to record 4 images

423 per hole except for initial test images.

424

425 **EM data processing and analysis**

426 Micrographs were corrected for beam-induced drift using patch motion and the contrast
427 transfer function (CTF) parameters for each micrograph were determined using Patch CTF in
428 cryoSPARC⁴³. 5527 movies were selected after curation for further processing. Early steps of
429 processing up to heterogeneous classification were carried out in two batches based on data
430 collection time. A simplified and summed representation of data processing is provided in Ext.
431 Data Fig. 1. Particles were picked with the blob picker function in cryoSPARC and subjected
432 to reference-free 2D classification. Ab initio reconstruction calculated on a subset of data (and
433 later refinement) revealed agreement with the previously determined BAM complex structure
434 5D0O (ref. 9). Heterogeneous refinement was done in three classes. Heterogeneity between the
435 classes was mainly observed for the POTRA domains. The class with the most structural
436 features was used for non-uniform refinement⁴³, particle box sizes were optimized by re-
437 extraction and non-uniform-homogeneous refinement, followed by local refinement using an
438 automatically determined global mask, which resulted in a reconstruction at 3.1 Å resolution.
439 Using global and local CTF refinement followed by two additional rounds of non-uniform and
440 local refinements, a final map at a global resolution of 3.0 Å was obtained. Modelling started
441 by manual fitting of subunits of the BamABCDE crystal structure (5D0O.pdb)⁹ into the EM
442 density map in UCSF Chimera⁴⁴. Model building was performed in Coot³⁷ and real-space
443 refinement was carried out in PHENIX^{39,45}. Validation was done using the cryo-EM validation
444 tools in PHENIX^{39,45}. The map resolution range was determined from local resolution
445 calculation in Cryosparc, and the model resolution range was determined calculating a map at
446 6 Å resolution in Chimera from the final model. This map was converted into a mask by

447 thresholding and applied to the local resolution map, to obtain the histogram of local resolution
448 in the model region.

449

450 **NMR spectroscopy**

451 Protein samples for NMR spectroscopy were expressed in M9 medium, supplemented with
452 perdeuterated water and 1 g/l ¹⁵N-ammonium chloride. Samples in 20 mM NaPi pH 7.5, NaCl
453 150 mM, 0.1% w/v LDAO were concentrated to a concentration of 300 μM. 2D [¹⁵N, ¹H]-
454 TROSY experiments were measured on a 700 MHz Bruker spectrometer equipped with a
455 cryogenic probe. 128 transients were accumulated at a sample temperature of 37 °C with 2048
456 and 256 complex points in the ¹H and ¹⁵N dimensions, respectively. The data were processed
457 using Topspin and analysed using ccpnmr⁴⁶. Chemical shift perturbation of the amide group
458 was calculated as:

$$459 \quad \Delta\delta(\text{HN}) = \sqrt{\Delta\delta_H^2 + (0.14 \cdot \Delta\delta_N^2)}$$

460 $\Delta\delta_H$ is the difference in the ¹H chemical shift of darobactin bound BamA-β and apo/nanobody
461 bound BamA-β. $\Delta\delta_N$ is the difference in the ¹⁵N chemical shift of darobactin bound BamA-β
462 and apo/nanobody bound BamA-β.

463

464 **Isothermal titration calorimetry**

465 The isothermal titration calorimetry experiments of darobactin binding to BamA-β variants
466 were carried out at 25°C with the Microcal ITC200 instrument in duplicates. BamA-β (100
467 μM) in 20 mM NaPi, 150 mM NaCl, 0.1% w/v LDAO, pH 7.5 was placed in the sample cell
468 and 1 mM darobactin in the same buffer was placed in the syringe. Successive 20 injections of
469 darobactin with a spacing of 120 s with a stirring rate of 500 rpm were introduced into the
470 protein solution. Reference experiments in the absence of BamA-β were carried out under
471 identical conditions. The resulting data were analyzed and fit to the independent binding model

472 using AFFINImeter web, with standard errors determined by Jackknife resampling⁴⁷. The direct
473 binding and competition experiments of β -signal peptides were done with 60 μ M BamA- β and
474 500 μ M darobactin. The competition data was fit globally with the constrained parameters K_D
475 and $\Delta H^{\text{binding}}$ for darobactin, and for each peptide with the free parameters K_D , $\Delta H^{\text{binding}}$,
476 darobactin concentration correction and heat of dilution. The 95% confidence interval was
477 calculated by error-surface projection, using the Fisher F-test in the software Sedphat^{48,49}.

478

479 ***In vivo* complementation assay**

480 The *in vivo* functionality of all BamA β -barrel mutants were tested in JCM166 cells. The cells
481 were transformed to contain full-length BamA in a pET3b plasmid. The full-length BamA
482 construct has an N-terminal His10-tag which was mutated to the respective single point
483 mutants. In JCM166 cells, the genomic gene of BamA is under control of an arabinose
484 promoter. In the presence of 0.1% L-(+)-arabinose, the BamA gene is expressed and the cells
485 show a normal phenotype. The absence of arabinose is lethal and cells only survive by
486 transformation with a BamA plasmid which is able to complement native BamA function.
487 pET3b with BamA⁺⁹ plasmid and pET3b with wild type BamA were used as negative¹⁵ and
488 positive control, respectively. All transformations were streaked out on agar plates without and
489 with 0.1% L-(+)-arabinose and incubated at 37 °C overnight.

490

491 **Mapping of conserved regions**

492 To map BamA β -barrel sequence conservation 103 full length BamA sequences
493 (Supplementary Table 8) were aligned with Clustal Omega⁵⁰. The alignment was manually
494 truncated to remove POTRA domains. The final alignment was used as input for AL2CO⁵¹ to
495 map conservation onto the *E. coli* BamA β -barrel structure. For better visualization of the data,

496 the flexible loop of residues 680–697, which is not resolved in the crystal structure, was
497 arbitrarily modeled.

498

499 **Construction of *bamA* mutants in *E. coli* MG1655**

500 For *E. coli bamA* recombinant mutant 2, *bamA* fragment containing F394V, E435K, G443D
501 mutations from spontaneous-darobactin-resistant *E. coli* strain 2 was amplified by PCR using
502 the primers bamA-rec-F (5'-ACTATCTGGATCGCGGTTATGC-3') and bamA-rec-R (5'-
503 TTCACAGCAGTCTGGATACGAG-3'), and the transformation was performed as previously
504 described⁶. To construct DNA fragments containing the different *bamA* mutations, overlap
505 extension PCR was performed using the common primer pair bamA-rec-F/bamA-rec-R. The
506 different mutations were created using primer pairs mut-R/mut-F (5'-
507 GGTAGCTTCAACTTTGTTATTGGTTACGGTACTG-3'/5'-CAGTACCGTAACCAATA
508 ACAAAGTTGAAGCTACC-3' for G429V, 5'-GTTCCAGTTTAAACATCGTTAAAACCTG
509 GTAAGTG-3'/5'-CACTTACCAGGTTTTAACGATGTTAAACTGGAAC-3' for G807V,
510 5'-GGTACTACTACATTAGCGATTGGTTACGGTACTGAAAG-3'/5'-CGCTAATGTAG
511 TAGTACCGGTGTTGCGCTCTTTTACC-3' for GSFNFG>GTTTLA, 5'-GACCAGGTA
512 GAGTTCTCTATTGGTTACGGTACTGAAAG -3'/5'-AGAGAACTCTACCTGGTTCGGTG
513 TTGCGCTCTTTTACC-3' for GSFNFG > DQV EFS). 5'- GGTATTGGTTACGGTGCTGA
514 AAGTGGCGTGAG-3'/5'-CTCACGCCACTTTCAGCACCGTAACCAATACC-3' for
515 T434A, 5'- CTTCCAGGCTGGTGTGCCGCAGGATAACTGGTTAGG-3'/5- CC TAACCA
516 GTTATCCTGCGGCACACCAGCCTGGAAG-3' for Q445P). Genomic DNA from Q445P
517 was used as template to construct the double mutant T434A, Q445P. The triple mutant T434A,
518 Q445P, A705T was described previously⁶. For each mutation, two DNA fragments were
519 amplified using the *E. coli* MG1655 chromosome as template with primers bamA-rec-F/mut-
520 R and mut-F/bamA-rec-R. The resulting DNA fragments were joined together by PCR using

521 primers bamA-rec-F/bamA-rec-R, and used to transform electrocompetent cells of *E. coli*
522 MG1655-pKD46 for λ red recombination⁵². The transformation protocol was adapted from the
523 “Quick and Easy *E. coli* Gene Deletion Kit” (GeneBridges, Heidelberg), as described
524 previously⁶. The transformant clones were first selected on 2x MIC darobactin (8 $\mu\text{g ml}^{-1}$).
525 Several clones were then restreaked for resistance to darobactin (8 $\mu\text{g ml}^{-1}$), as well as
526 sensitivity to ampicillin (100 $\mu\text{g ml}^{-1}$, at 30 °C). Each mutation in *bamA* was confirmed via
527 sequencing of the *bamA* locus. The MIC of darobactin against the *E. coli* MG1655 and *bamA*
528 mutants was determined by microbroth dilution, as previously described⁶.

529

530 **Construction of the Bam diploid mutants and growth inhibition assay**

531 The plasmids carrying Bam with wild type or mutated BamA (pBAM-WT, no mutation;
532 pBAM-M2, F394V, E435K and G443D; pBAM-M3, T434A, Q445P and A705T) were used
533 for this study⁶. Plasmids were transformed into *E. coli* MG1655, *bamA* recombinant mutant 2
534 (F394V, E435K and G443D), mutant 3 (T434A, Q445P and A705T) *bamA6* mutant, *bamA66*
535 mutant or *bamA101* mutant by electroporation⁵³⁻⁵⁵. Strains were inoculated into Mueller-
536 Hinton II broth (MHIIB) with (for mutants with plasmid which carry Bam) or without (parental
537 strain) 50 $\mu\text{g ml}^{-1}$ of ampicillin at 37 °C with aeration at 220 rpm. After overnight cultivation,
538 bacterial culture was diluted 1:100 in MHIIB with or without 50 $\mu\text{g ml}^{-1}$ of ampicillin and 0.1
539 mM of IPTG and incubated at 37 °C with aeration at 220 rpm. Exponential culture (OD₆₀₀ of
540 0.2–0.3) was diluted to an OD₆₀₀ of 0.001 (approximately 5×10^5 c.f.u. ml^{-1}) in MHIIB with
541 or without 50 $\mu\text{g ml}^{-1}$ of ampicillin and 0.1 mM of IPTG. 98 μl aliquots were transferred into
542 round-bottom 96 well plates containing 2 μl of darobactin diluted serially twofold. After
543 overnight cultivation at 37 °C, the MIC of darobactin was determined.

544

545 **Native mass spectrometry on the BAM complex**

546 BAM complex was overexpressed from plasmid pJH114 in BL21(DE3) cells (NEB), grown in
547 LB medium containing carbenicillin ($100 \mu\text{g ml}^{-1}$). When the culture reached an optical density
548 at 600 nm of ~ 0.5 , expression was induced with 0.5mM isopropyl β -thiogalactopyranoside
549 (IPTG) for 3h at 37 °C. Cells were pelleted by centrifugation at 5,000g and resuspended in a
550 buffer containing 50 mM Tris-HCl (pH 8.0), 300 mM NaCl and EDTA-free protease inhibitor
551 cocktail (Roche). The cells were then disrupted by a microfluidizer (Microfluidics). After
552 centrifugation (20,000 g for 20 min), the supernatant was filtered and loaded onto a 5 ml His
553 Trap-HP column in case of soluble proteins while for membrane proteins, the supernatant was
554 ultracentrifuged (200,000 g), and the membrane fractions were collected. The proteins were
555 solubilized from the membrane fraction with 20 mM Tris (pH 8.0), 150 mM NaCl, 20%
556 glycerol, 2% DDM (Anatrace) for 2 h at 4 °C. The insoluble material was removed by
557 ultracentrifugation. The supernatant was filtered before loading onto a 5 ml His Trap-HP
558 column (GE Healthcare) equilibrated in 20 mM Tris (pH 8.0), 150 mM NaCl, 20 mM
559 imidazole, 10% glycerol and 0.03% DDM. After the clarified supernatant was loaded, the
560 column was initially washed with 50 ml of 20 mM Tris (pH 8.0), 150 mM NaCl, 20 mM
561 imidazole, 10% glycerol and 0.03% DDM and washed again with 50 ml of 20 mM Tris (pH
562 8.0), 150 mM NaCl, 80 mM imidazole, 10% glycerol and 0.03% DDM. The bound protein was
563 then eluted with 20 mM Tris (pH 8.0), 150 mM NaCl, 300 mM imidazole, 10% glycerol and
564 0.03% DDM. Peak fractions were pooled, concentrated and injected onto a Superdex 200 GL
565 10/300 (GE Healthcare) column equilibrated in buffer 20 mM Tris (pH 8.0) and 150 mM NaCl,
566 and 0.5% C_8E_4 . Peak fractions were concentrated and was either used immediately or flash-
567 frozen in liquid nitrogen and stored at $-80 \text{ }^\circ\text{C}$.
568 Prior to MS analysis, the protein was buffer exchanged into 200 mM ammonium acetate pH
569 8.0 and 0.5% C_8E_4 using a Biospin-6 (BioRad) column and introduced directly into the mass

570 spectrometer using gold-coated capillary needles (prepared in-house). Data were collected on
571 a Q-Exactive UHMR mass spectrometer (Thermo Fisher Scientific). The instrument
572 parameters were as follows: capillary voltage 1.1 kV, S-lens RF 100%, quadrupole selection
573 from 1,000 to 20,000 m/z range, collisional activation in the HCD cell 300 V, trapping gas
574 pressure setting 7.5, temperature 200 °C, and resolution of the instrument 12,500. The noise
575 level was set at 3 rather than the default value of 4.64. No in-source dissociation was applied.
576 Data were analysed using Xcalibur 4.2 (Thermo Scientific) and UniDec⁵⁶ software packages.
577 Lipids and darobactin were diluted into a buffer containing 200 mM ammonium acetate pH 8.0
578 and 0.5% (w/v) C₈E₄ and were added in different ratios to solutions of Bam complex in the
579 same buffer. All experiments were repeated three times with similar outcome. Statistical
580 analysis was performed using Prism 8 software (GraphPad). Results are mean ± s.d., n
581 represents three independent experiments. Comparisons for two groups were calculated using
582 unpaired two-tailed Student's t-tests. Exact *P* values are indicated in the figures and in figure
583 legends where possible.

584

585 **Molecular dynamics simulations**

586 The experimentally solved BamA structure (residues 419-810) was assigned with
587 CHARMM36m⁵⁷ parameters at neutral pH. The BamA N-terminus was treated in the neutral,
588 deprotonated form, as part of the BAM complex. The C-terminus was negatively charged. The
589 darobactin parameters were assigned using CgenFF⁵⁸, also assuming neutral pH. BamA and
590 BamA-darobactin–membrane systems were built using the CHARMM-GUI membrane
591 builder⁵⁹. The orientation of BamA with respect to the membrane was predicted using the OPM
592 server⁶⁰. Each membrane inner leaflet corresponded to standard *E. coli* lipids⁶¹ in a 0.9:0.05:0.5
593 ratio for palmitoyl-oleoyl-phosphatidyl-ethanolamine (PE), palmitoyl-oleoyl-phosphatidyl-
594 glycerol (PG), and cardiolipin (CL), respectively. The outer leaflet was made of R1-type core

595 LPS, the most frequent among *E. coli* strains. Each simulation box had a dimension of
596 $\sim 10 \times 10 \times 10 \text{ nm}^3$ which resulted in 48 LPS molecules in the outer leaflet and 126 PE, 7 PG and
597 7 CL lipid molecules in the inner leaflet. Subsequently, the box was filled with $\sim 21,000$
598 TIP3P⁶² water molecules. The overall charge of each system was neutralized by the addition
599 of $\sim 150 \text{ mM}$ magnesium chloride. Energy minimization using steepest descents was performed
600 for $\leq 5,000$ steps with a 0.1 nm step size. Equilibrations in the NVT and NPT ensembles were
601 performed for $\sim 100 \text{ ns}$ in total with position restraints on BamA or BamA-darobactin heavy
602 atoms, while no restraints were applied to the membrane or solvent. In total, 5 membrane
603 systems were prepared: i) BamA in the darobactin free (apo) state; ii) BamA-darobactin
604 complex; iii) Strain 1: G429V, G807V mutations; iv) Strain 2: F394, E435K, G443D
605 mutations; and v) Strain 3: T434A, Q445T, A705T mutations. All in silico point mutations
606 were performed using CHARMM-GUI. All unrestrained production simulations were run in
607 the NPT ensemble in triplicate with different starting velocities for $1 \mu\text{s}$ each, using
608 GROMACS2018⁶¹. Equations of motion were integrated through the Verlet leapfrog algorithm
609 with a 2 fs time step, and bonds connected to hydrogens were constrained with the LINCS
610 algorithm. The cutoff distance was 1.2 nm for the short-range neighbor list and van der Waal's
611 interactions with a smooth switching function from 1.0 nm . The Particle Mesh Ewald method
612 was applied for long-range electrostatic interactions with a 1.2 nm real space cutoff⁶³. The
613 Nose-Hoover thermostat^{64,65} and Parinello-Rahman barostat⁶⁶ were used to maintain the
614 temperature and pressure at 310 K and 1 bar , respectively. Simulations were performed on: i)
615 an in-house Linux cluster composed of 7 nodes containing 2 GPUs (Nvidia GeForce RTX 2080
616 Ti) and 24 CPUs (Intel® Xeon® Gold 5118 CPU @ 2.3 GHz) each; and ii) ASPIRE 1, the
617 petascale cluster at the Singapore National Supercomputing Centre, where each simulation
618 employed 4 nodes each consisting of 1 GPU (Nvidia Tesla K40t) and 24 CPUs (Intel® Xeon®
619 CPU E5-2690 v3 @ 2.6 GHz). Partial densities were calculated using *g_mydensity* over the

620 entire 3 μ s sampling per system⁶⁷. The number of contacts was calculated based on a 0.3 nm
621 cutoff distance for the entire 3 μ s of sampling per system. The most dominant conformations
622 were clustered on protein heavy atoms using the Gromos method with a root mean square
623 deviation (RMSD) cutoff distance of 0.35 nm. The percentage of the darobactin molecule
624 exposed to either water, lipids, or protein was calculated based on its solvent accessible surface
625 and averaged over the entire trajectory.

626

627 **Analysis of β -signal sequences**

628 To identify a set of β -signals we followed a modified version of the procedure established by
629 Paramsivam et al., 2012⁶⁸. A total of \sim 860,000 sequences of outer membrane β -barrel proteins
630 were obtained from the OMPdb (database release Dec 1, 2020)⁶⁹. The prokaryotic sequences
631 were retained and filtered for non-redundancy towards a pairwise identity $<$ 90%. Out of these,
632 only sequences associated with a topology prediction with reliability larger than 80% were
633 kept. For each remaining sequence, the last β -strand in the topology prediction was selected
634 and subjected to the following rules: (1) If its C-terminus corresponded to the protein C-
635 terminus, the 10 C-terminal residues were kept. (2) Otherwise, the sequence was extended
636 towards the protein C-terminus until an aromatic residue was found, but by maximally 4
637 residues. The 10 C-terminal residues were kept. (3) If no aromatic residue was found, the last
638 β -strand was extended to the protein C-terminus and the first 10-residue long sequence portion
639 that matches the regular expression of Paramsivam et al was selected. Sequences were removed
640 if no matches to the regular expression were found. The final set of " β -signals" contained
641 263,003 sequences.

642 To compare the darobactin sequence to the set of β -signals by amino acid type, a position-
643 specific frequency matrix (PSFM) and a position-specific scoring matrix (PSSM) were
644 generated from the β -signals set. Then, the PSSM was used to calculate the log-likelihood score

645 for each sequence in: (1) the β -signals set (“ β -signal sequences”, 263,003 entries); (2) an
646 equally large set of 7-residue long, randomly generated amino acid sequences (“random
647 sequences”, 263,003 entries); (3) a set of unique permutations of the darobactin sequence
648 (“darobactin sequence permutations”, 1,260 entries). The score of darobactin was compared to
649 scores of sets 1–3 using percentiles. The same type of analysis was also done by amino acid
650 chemistry, a position-specific count matrix (PSCM) was generated from the β -signals
651 according to their chemistry: STNQY, polar non-charged; DEKRH, charged; G, Neutral;
652 AVCPLIMWF, Hydrophobic and non-polar; FWY, aromatic. Then, new PSFM and PSSM
653 were generated from the PSCM. Any amino acid sequence was converted to the best scoring
654 chemistry sequence in accordance with the new PSSM. Figure panels were created with
655 matplotlib and logomaker^{70,71}.
656

657 **References**

658

659 33 Kaur, H., Grahl, A., Hartmann, J. B. & Hiller, S. Sample preparation and technical setup
660 for NMR spectroscopy with integral membrane proteins. *Methods Mol Biol* **2127**, 373-
661 396, (2020).

662 34 Kabsch, W. Xds. *Acta Crystallogr D Biol Crystallogr* **66**, 125-132, (2010).

663 35 Evans, P. R. & Murshudov, G. N. How good are my data and what is the resolution?
664 *Acta Crystallogr D Biol Crystallogr* **69**, 1204-1214, (2013).

665 36 McCoy, A. J. *et al.* Phaser crystallographic software. *J Appl Crystallogr* **40**, 658-674,
666 (2007).

667 37 Emsley, P. & Cowtan, K. Coot: model-building tools for molecular graphics. *Acta*
668 *Crystallogr D Biol Crystallogr* **60**, 2126-2132, (2004).

669 38 Schuttelkopf, A. W. & van Aalten, D. M. PRODRG: a tool for high-throughput
670 crystallography of protein-ligand complexes. *Acta Crystallogr D Biol Crystallogr* **60**,
671 1355-1363, (2004).

672 39 Adams, P. D. *et al.* PHENIX: building new software for automated crystallographic
673 structure determination. *Acta Crystallogr D Biol Crystallogr* **58**, 1948-1954, (2002).

674 40 Chen, V. B. *et al.* MolProbity: all-atom structure validation for macromolecular
675 crystallography. *Acta Crystallogr D Biol Crystallogr* **66**, 12-21, (2010).

676 41 DeLano, W. L. J. C. N. O. P. C. Pymol: An open-source molecular graphics tool. **40**,
677 82-92, (2002).

678 42 Mastronarde, D. N. Automated electron microscope tomography using robust
679 prediction of specimen movements. *J Struct Biol* **152**, 36-51, (2005).

680 43 Punjani, A., Rubinstein, J. L., Fleet, D. J. & Brubaker, M. A. cryoSPARC: algorithms
681 for rapid unsupervised cryo-EM structure determination. *Nat Methods* **14**, 290-296,
682 (2017).

683 44 Pettersen, E. F. *et al.* UCSF Chimera--a visualization system for exploratory research
684 and analysis. *J Comput Chem* **25**, 1605-1612, (2004).

685 45 Afonine, P. V. *et al.* Real-space refinement in PHENIX for cryo-EM and
686 crystallography. *Acta Crystallogr D Struct Biol* **74**, 531-544, (2018).

687 46 Vranken, W. F. *et al.* The CCPN data model for NMR spectroscopy: development of a
688 software pipeline. *Proteins* **59**, 687-696, (2005).

689 47 Pineiro, A. *et al.* AFFINImeter: A software to analyze molecular recognition processes
690 from experimental data. *Anal Biochem* **577**, 117-134, (2019).

691 48 Kemmer, G. & Keller, S. Nonlinear least-squares data fitting in Excel spreadsheets. *Nat*
692 *Protoc* **5**, 267-281, (2010).

693 49 Zhao, H., Piszczek, G. & Schuck, P. SEDPHAT--a platform for global ITC analysis
694 and global multi-method analysis of molecular interactions. *Methods* **76**, 137-148,
695 (2015).

696 50 Sievers, F. *et al.* Fast, scalable generation of high-quality protein multiple sequence
697 alignments using Clustal Omega. *Mol Syst Biol* **7**, 539, (2011).

698 51 Pei, J. & Grishin, N. V. AL2CO: calculation of positional conservation in a protein
699 sequence alignment. *Bioinformatics* **17**, 700-712, (2001).

700 52 Datsenko, K. A. & Wanner, B. L. One-step inactivation of chromosomal genes in
701 *Escherichia coli* K-12 using PCR products. *Proc Natl Acad Sci USA* **97**, 6640-6645,
702 (2000).

703 53 Bennion, D., Charlson, E. S., Coon, E. & Misra, R. Dissection of β -barrel outer
704 membrane protein assembly pathways through characterizing BamA POTRA 1 mutants
705 of *Escherichia coli*. *Mol Microbiol* **77**, 1153-1171, (2010).

706 54 Ruiz, N., Wu, T., Kahne, D. & Silhavy, T. J. Probing the barrier function of the outer
707 membrane with chemical conditionality. *ACS Chem Biol* **1**, 385-395, (2006).

708 55 Aoki, S. K. *et al.* Contact-dependent growth inhibition requires the essential outer
709 membrane protein BamA (YaeT) as the receptor and the inner membrane transport
710 protein AcrB. *Mol Microbiol* **70**, 323-340, (2008).

711 56 Marty, M. T. *et al.* Bayesian deconvolution of mass and ion mobility spectra: from
712 binary interactions to polydisperse ensembles. *Anal Chem* **87**, 4370-4376, (2015).

713 57 Huang, J. *et al.* CHARMM36m: an improved force field for folded and intrinsically
714 disordered proteins. *Nat Methods* **14**, 71-73, (2017).

715 58 Vanommeslaeghe, K. *et al.* CHARMM general force field: A force field for drug-like
716 molecules compatible with the CHARMM all-atom additive biological force fields. *J*
717 *Comput Chem* **31**, 671-690, (2010).

718 59 Jo, S., Kim, T., Iyer, V. G. & Im, W. CHARMM-GUI: a web-based graphical user
719 interface for CHARMM. *J Comput Chem* **29**, 1859-1865, (2008).

720 60 Lomize, M. A., Pogozheva, I. D., Joo, H., Mosberg, H. I. & Lomize, A. L. OPM
721 database and PPM web server: resources for positioning of proteins in membranes.
722 *Nucleic Acids Res* **40**, D370-376, (2012).

723 61 Van Der Spoel, D. *et al.* GROMACS: fast, flexible, and free. *J Comput Chem* **26**, 1701-
724 1718, (2005).

725 62 Jorgensen, W. L., Chandrasekhar, J., Madura, J. D., Impey, R. W. & Klein, M. L.
726 Comparison of simple potential functions for simulating liquid water. *J Chem Phys* **79**,
727 926-935, (1983).

728 63 Essmann, U. *et al.* A smooth particle mesh Ewald method. *J Chem Phys* **103**, 8577-
729 8593, (1995).

730 64 Hoover, W. G. Canonical dynamics - equilibrium phase-space distributions. *Phys Rev*
731 *A* **31**, 1695-1697, (1985).

732 65 Nose, S. A Unified formulation of the constant temperature molecular-dynamics
733 methods. *J Chem Phys* **81**, 511-519, (1984).

734 66 Parrinello, M. & Rahman, A. Polymorphic transitions in single crystals - a new
735 molecular-dynamics method. *J Appl Phys* **52**, 7182-7190, (1981).

736 67 Castillo, N., Monticelli, L., Barnoud, J. & Tieleman, D. P. Free energy of WALP23
737 dimer association in DMPC, DPPC, and DOPC bilayers. *Chem Phys Lipids* **169**, 95-
738 105, (2013).

739 68 Paramasivam, N., Habeck, M. & Linke, D. Is the C-terminal insertional signal in Gram-
740 negative bacterial outer membrane proteins species-specific or not? *BMC Genomics* **13**,
741 510, (2012).

742 69 Tsirigos, K. D., Bagos, P. G. & Hamodrakas, S. J. OMPdb: a database of β -barrel outer
743 membrane proteins from Gram-negative bacteria. *Nucleic Acids Res* **39**, D324-331,
744 (2011).

745 70 Hunter, J. D. Matplotlib: A 2D graphics environment. *Comput Sci Eng* **9**, 90-95, (2007).

746 71 Tareen, A. & Kinney, J. B. Logomaker: beautiful sequence logos in Python.
747 *Bioinformatics* **36**, 2272-2274, (2020).

748

749 **Data Availability**

750 The data that support the findings of this study are available from the corresponding author
751 upon request. The atomic coordinates have been deposited in the RCSB Protein Data Bank and
752 are available under the accession codes 7NRE and 7NRF. The cryo-EM map has been
753 deposited in the Protein Data Bank under accession code 7NRI and EMDB accession code
754 12546. Mass spectrometry data has been deposited in figshare with DOI:
755 10.6084/m9.figshare.12179784. For the study, data was retrieved from the OMPdb (release
756 Dec 1, 2020).

757

758 **Acknowledgements**

759 We thank Harris Bernstein and Christoph Bieniossek for expression plasmids, Tim Sharpe,
760 Thomas Müntener and the Biozentrum Bio-EM lab for scientific support and discussions. The
761 scientific computing center at University of Basel (sciCORE) and the National
762 Supercomputing Centre Singapore (NSCC) are acknowledged for providing computational
763 resources. This work was supported by the Swiss National Science Foundation (grants 167125,
764 185388 and 187170 to S.H. and R'Equip 177084 to T.M.), AntiResist: New approaches to
765 combat antibiotic-resistant bacteria (51AU40_180541), the Medical Research Council
766 (program grant MR/N020413/1 awarded to C.V.R), the Bioinformatics Institute (BII) A*STAR
767 and NRF (NRF2017NRF-CRP001-027 to P.J.B. and J.K.M.), and by the NIH (grant P01
768 AI118687 to K.L.).

769

770 **Author contributions**

771 CVR, KL, TM and SH designed the study and supervised experiments. RG and YI performed
772 the microbiology experiments. JRB performed the mass-spec experiments. HK and RPJ
773 performed all other experiments. JKM and PJB ran simulations. EA performed sequence

774 analysis. All authors analyzed data and discussed the findings. HK, KL, TM and SH wrote the
775 manuscript. All authors edited and approved the manuscript.

776

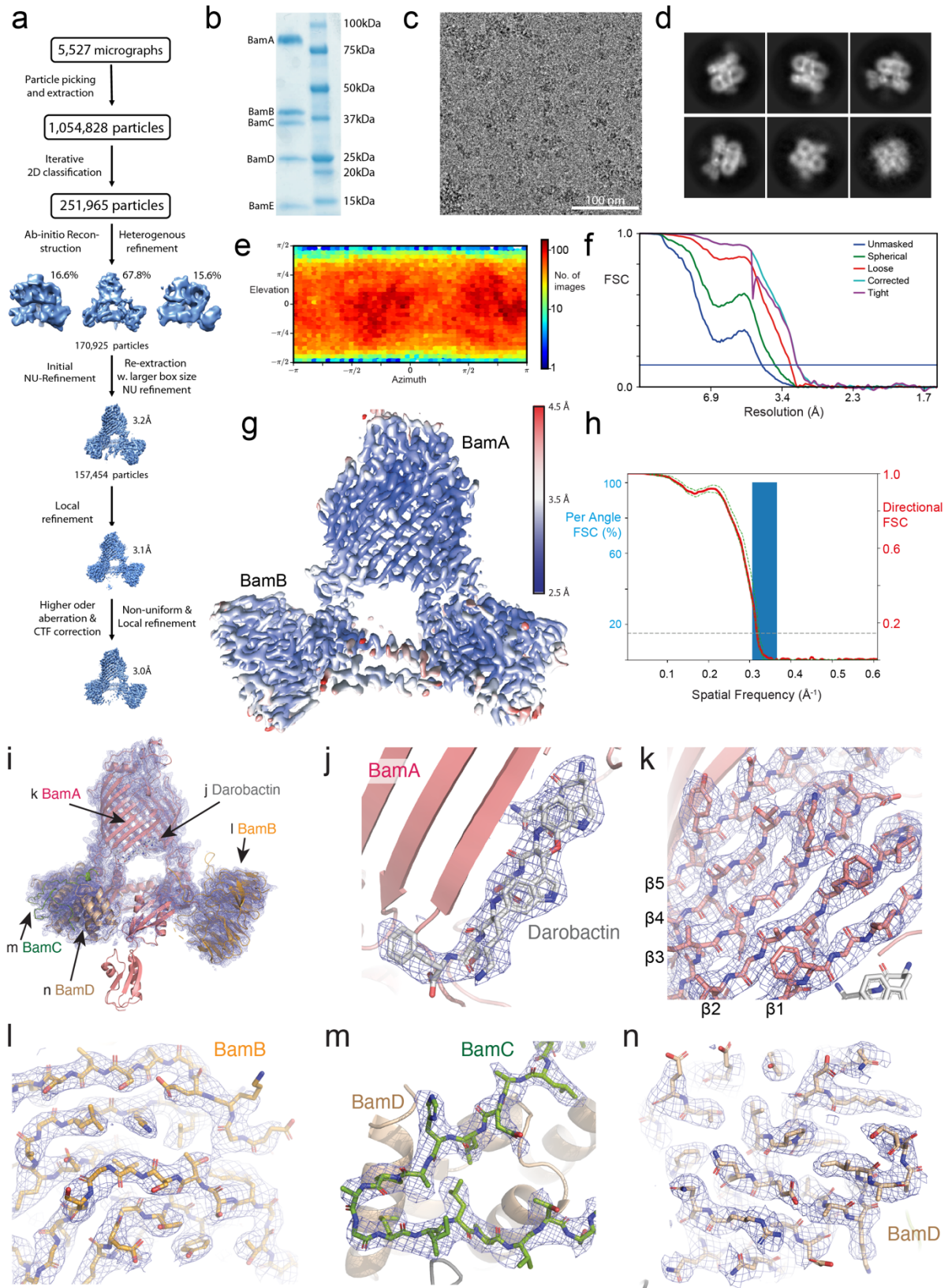
777 **Declaration of interest**

778 The authors declare that they do not have competing financial interests.

779

780 **Supplementary Information** is available for this paper.

781

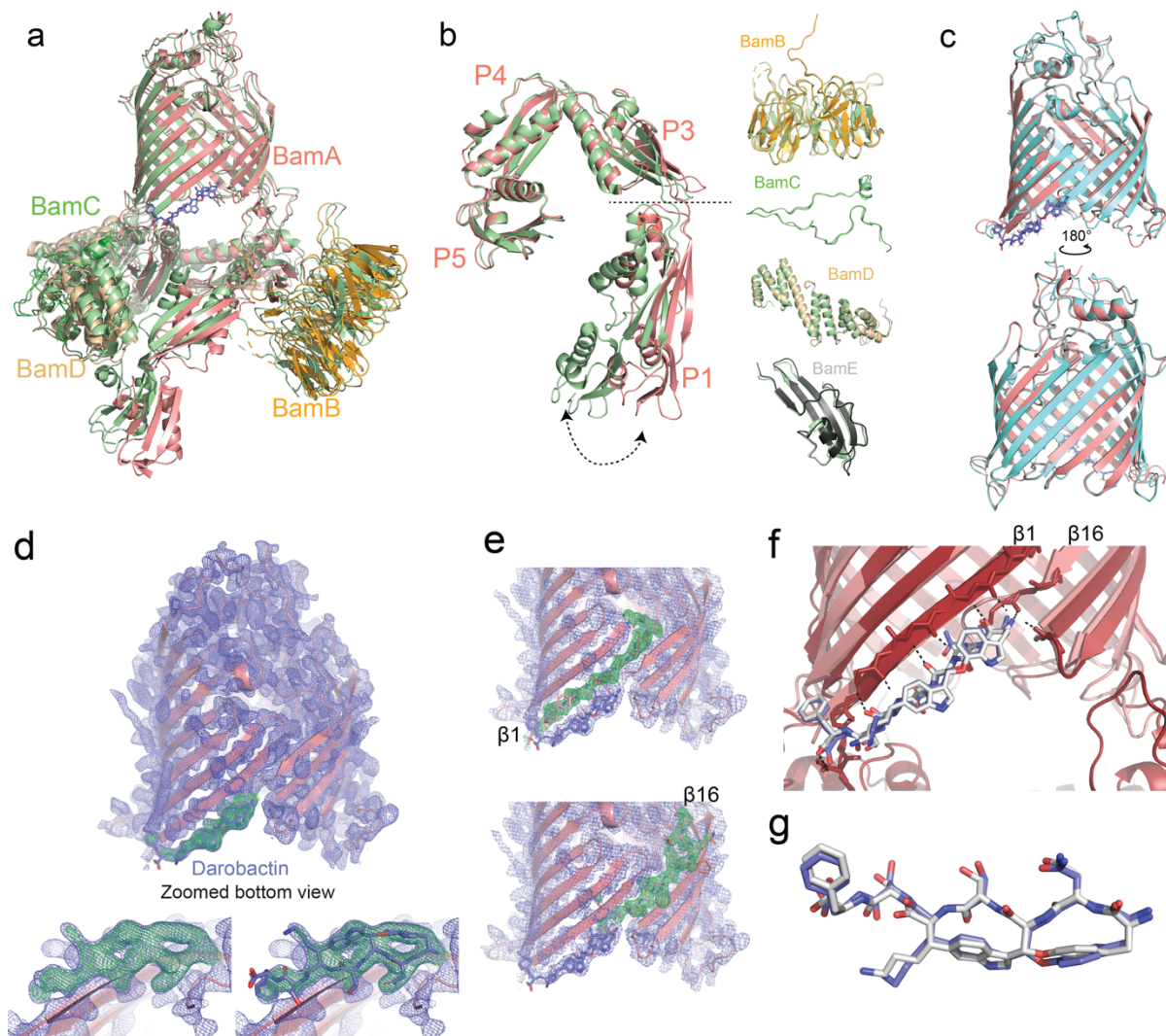


783

784 **Extended Data Fig. 1. Cryo-electron microscopy structure of the BAM–darobactin**785 **complex.** (a) Flow chart of data processing to generate the structure, see Methods for details.

786 (b) Purified BAM–darobactin sample used for cryo-EM structure determination analyzed on
787 SDS-PAGE. This experiment was repeated at least three times independently with similar
788 results. (c) Representative electron micrograph of BAM–darobactin. This experiment was
789 repeated at least three times independently with similar results. (d) Selected examples of 2D
790 classes from cryoSPARC. (e) Viewing direction distribution plot for the final three-
791 dimensional reconstruction (f) FSC curves for unmasked, spherically, loose and tight masks
792 and corrected FSC curve for the final reconstruction. (g) Local resolution variations of the EM
793 reconstruction, with coloring as indicated. POTRA domains 1 and 2 are at a local resolution
794 below 4.5 Å and are only visualized at lower contour level where micelle density obscures the
795 view onto the BamA barrel. (h) Plot of directional FSC (red) and histogram of per angle FSC
796 (blue) and ± 1 S.D from mean of the directional FSC. FSC curve indicates a resolution of 3.15
797 Å. (i) Overview of the cryo-EM reconstruction of the BAM complex. BAM is shown in ribbon
798 representation, the coulomb potential map as blue mesh. Note that the density of POTRA
799 domains P1 and P2 is below the display threshold chosen here due to motional averaging. (j–
800 n) Zoomed local views, showing the map around selected atoms in stick representation from
801 the directions and viewpoints indicated by arrows and letters in i.

802



803

804 **Extended Data Fig. 2. Structural details of the cryo-EM and crystal structures of BAM.**

805 (a) Superposition of the BAM–darobactin cryo-EM structure (salmon) with the ligand-free

806 BAM crystal structure (green, PDB 5D0O). (b) Superposition of POTRA domains P1–P5 and

807 the individual components BamB–BamE, as indicated. The dashed horizontal line indicates the

808 pivot between P2 and P3 around which P1 and P2 are rotated by rigid-body movement. (c)

809 Superposition of the BamA-β barrel–darobactin crystal structure (salmon) with a closed gate

810 BamA-β barrel crystal structure (cyan, PDB 4N75). (d) Crystallographic omit map for

811 darobactin bound at the lateral gate region of the BamA β-barrel after refinement of the model

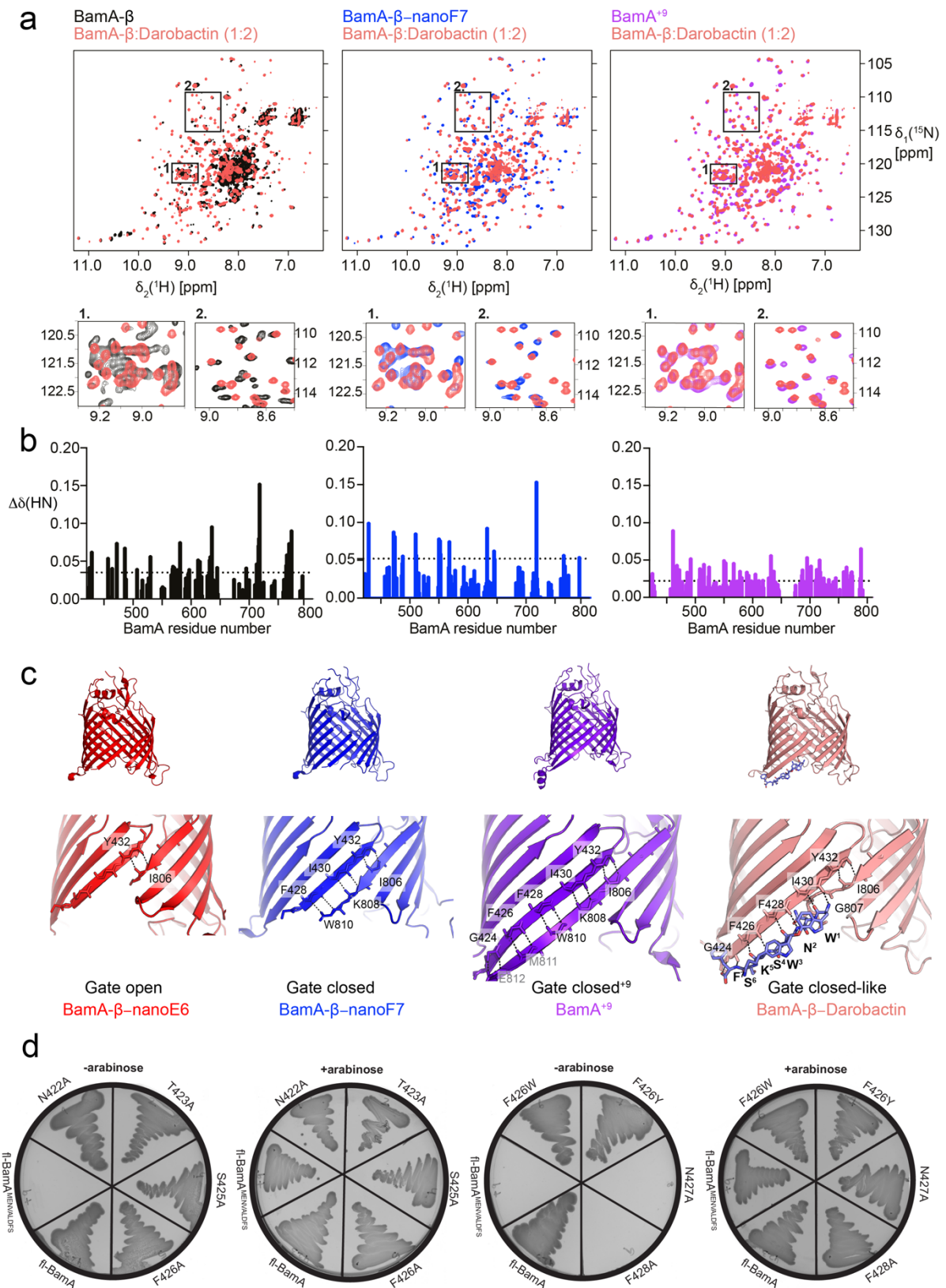
812 without darobactin. The $2mF_o-DF_c$ map is shown at 1σ in slate and the mF_o-DF_c difference813 map at $\pm 3\sigma$ level in green and red. Top: Overview of an entire BamA barrel, bottom left and

814 right: zoom in without and with overlay of the refined model coordinates. The cyclizations of
815 darobactin can clearly be observed at 2.3 Å resolution. (e) Omit map for strands β 1 (top) and
816 β 16 (bottom) of the BamA β -barrel visualized as in panel d. (f) Superposition of the cryo-EM
817 and X-ray structures. X-ray structure is colored salmon/blue for BamA/darobactin. Cryo-EM
818 structure bordeaux/white. (g) Same for the ligand darobactin only.

819

820

821

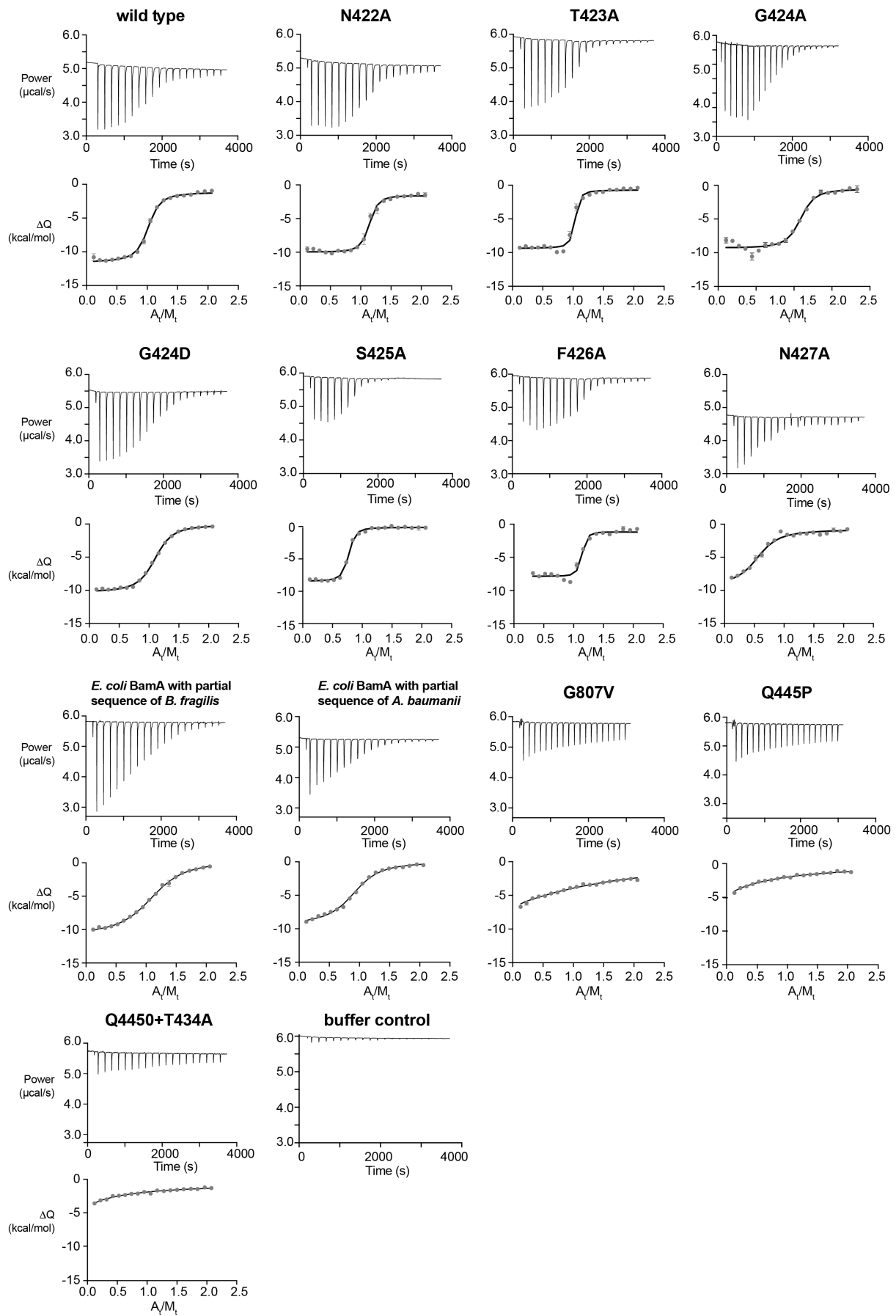


822
823

824 **Extended Data Fig. 3. Comparison of BamA β -barrel conformations in aqueous solution. (a)**

825 **Comparison of 2D [^{15}N , ^1H]-TROSY fingerprint spectra of different BamA preparations in LDAO.**

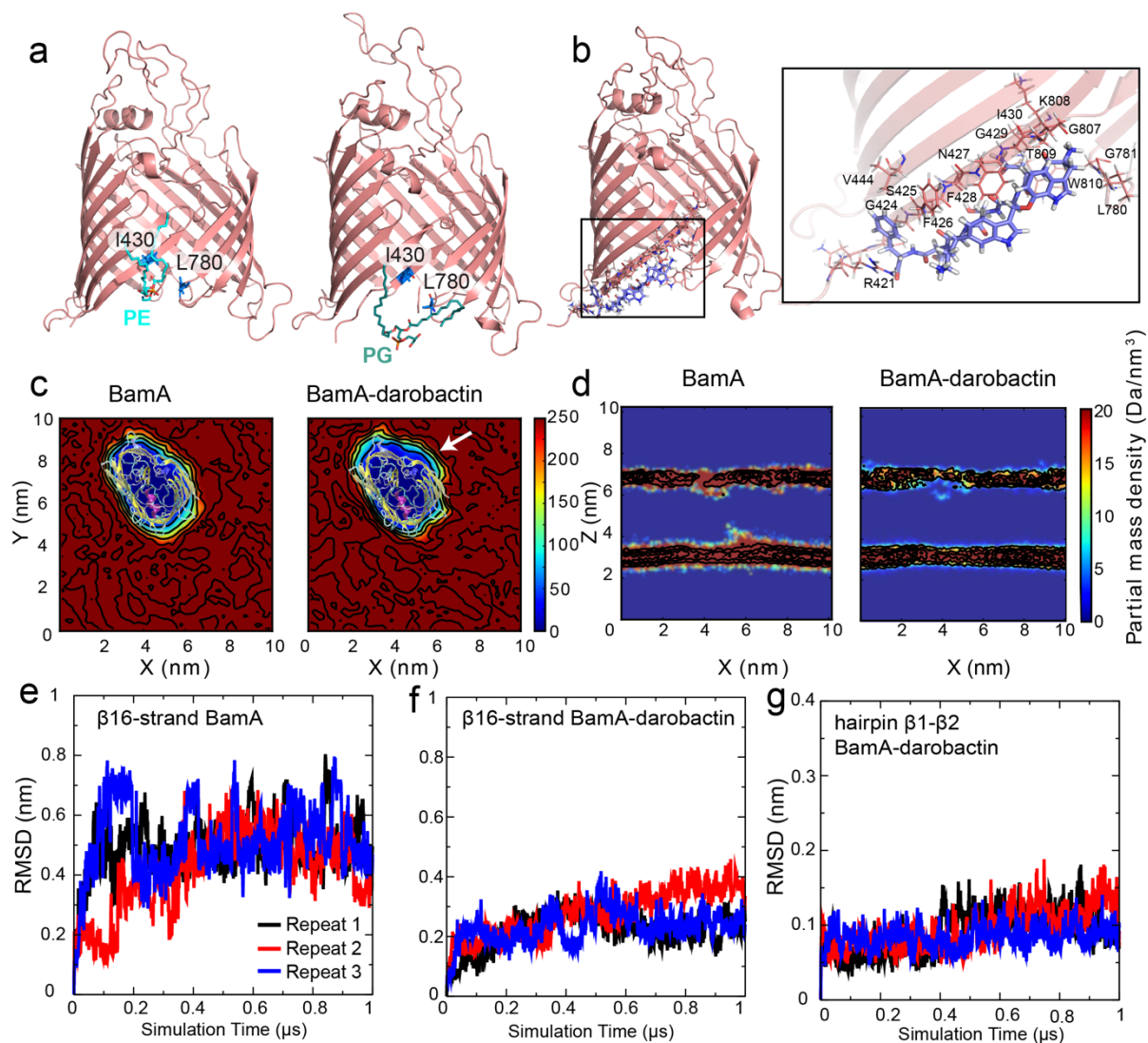
826 Left: Overlay of BamA- β fingerprint spectra in the absence and presence of darobactin.
827 Middle: Overlay of fingerprint spectra of BamA- β -nanobodyF7 and BamA- β -darobactin.
828 Right: Overlay of fingerprint spectrum of BamA⁺⁹ and BamA- β -darobactin complex. Bottom
829 panels show zoomed regions of the spectra. (b) Backbone amide chemical shift perturbations
830 between the fingerprint spectrum of BamA- β with and without darobactin (left, black), Bam-
831 β -nanobodyF7 in comparison with BamA-darobactin (middle, blue) and BamA⁺⁹ in
832 comparison with BamA-darobactin (right, purple). The dotted lines indicate the average CSP,
833 which can be interpreted as a measure of dissimilarity between two spectra. (c) Structures of
834 BamA- β barrel in various conformations of the gate region. Bottom panel shows zoomed in
835 part of the backbone with H-bonds between β 1 and β 16 or darobactin indicated. From left
836 to right: open gate (6QGW, red), closed gate (6QGX, blue) and BamA⁺⁹ (6FSU, purple) and
837 BamA-darobactin complex. (d) *In vivo* functional assay of BamA barrel mutants and C-terminal
838 extensions using JCM166 cells in the absence and presence of arabinose. fl-BamA^{MENVALDFS}
839 and fl-BamA serve as a negative and positive control, respectively.
840



842 **Extended Data Fig. 4. Isothermal titration calorimetry (ITC) of BamA- β barrel in**
843 **detergent micelles and its variants titrated with darobactin.** Experiments were repeated
844 independently twice with similar results.

845

846
847

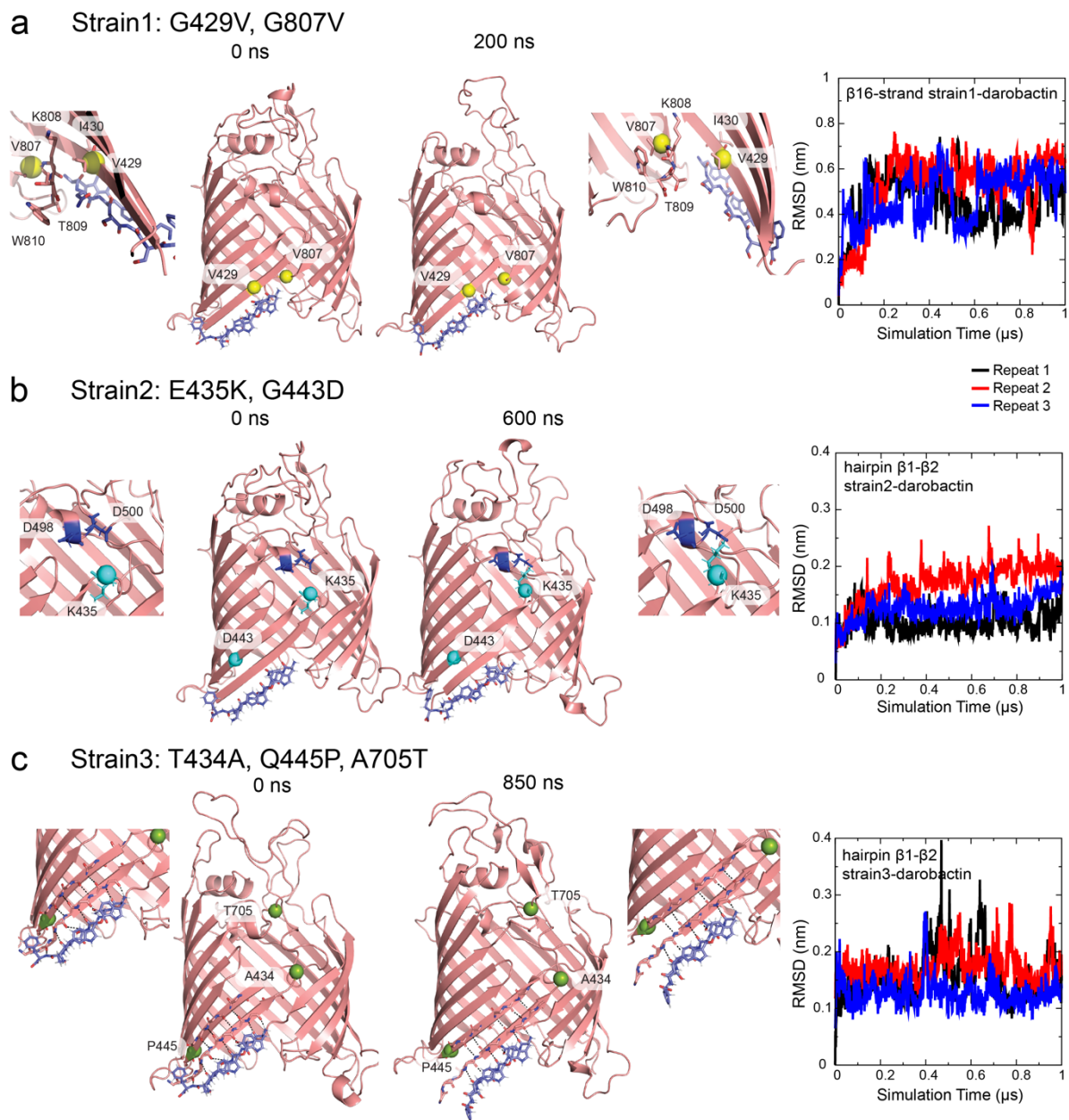


848

849 **Extended Data Fig. 5. MD simulations of BamA-β barrel.** (a) Representative snapshots of
850 lipid PE molecule (left) and PG molecule (right) anchored by Ile430 and Leu780 in the gate
851 region. (b) The most dominant conformation of BamA–darobactin complex showing contacts
852 consistently observed between BamA-β barrel and darobactin throughout the simulation
853 sampling. (c) Partial densities of all lipids (top-down view of the membrane); the white arrow
854 highlights the darobactin-binding region. (d) Partial densities of lipid phosphate groups (side-
855 view of the membrane). (e–g) Structural drift and fluctuations of key β-strands around the
856 darobactin binding site. Time-dependent root mean square deviation (RMSD) measured with

857 respect to the initial structure for backbone atoms of β -strands, after performing a least-squares
858 fit. The resulting RMSD is shown for: (e) β 16 in ligand-free BamA, (f) β 16 in BamA–
859 darobactin complex, (g) hairpin β 1/ β 2 in BamA–darobactin complex.

866 intensities of lipid binding peaks from (a) suggest that the negatively charged PG and CL have
867 higher affinity. (d) Mass spectra of BAM complex with lipids and darobactin. Bottom spectra
868 with PE and darobactin, and top spectra with PG and darobactin. Zoom in a section of the 23+
869 charge state highlights the bound peaks and relative ratio of darobactin binding is shown in bar
870 charts. No significant increase in darobactin binding is observed in these two cases, suggesting
871 that PE and PG lipids do not affect darobactin binding. (e) Mass spectra of BAM complex with
872 lipid mixtures (PE+CL, bottom spectra and PG+CL, top spectra) and darobactin. Lipids,
873 darobactin and their various combination binding peaks are highlighted in the zoom-in section
874 for the charge state 23+. Bar charts of relative peak intensities indicate that darobactin bound
875 with CL is observed to a greater extent than bound alone and PE and PG bound in both cases.
876 This increase is even higher for 2xCL bound species and is slightly lower for PE or PG bound
877 to 1xCL species. However, no change in darobactin binding is observed for PE and PG. The
878 mean relative binding intensities are significantly different in the different lipid-bound forms
879 and are highlighted in bar charts. Bars (c-e) represent mean \pm s.d., points show data from three
880 independent experiments. * $P < 0.05$; ** $P < 0.01$; *** $P < 0.001$; NS, not significant; two-tailed
881 unpaired Student's t-test. Exact P values are indicated in the figures.
882



883

884 **Extended Data Fig. 7. MD Simulations of the effect of darobactin-resistance mutations**

885 **on the BamA–darobactin interaction.** (a) Representative snapshots with zoomed views from

886 a simulation with strain 1 bound to darobactin. Mutations G429V and G807V are shown as

887 yellow spheres at the α -carbon position. Time-dependent root mean square deviation (RMSD)

888 of β 16 backbone atoms relative to the initial structure. (b) Same for strain 2 (mutations E435K

889 and G443D, cyan) and RMSD of hairpin β 1/ β 2. (c) Same for strain 3 (mutations T434A,

890 Q445P, A705T, green) and RMSD of hairpin β 1/ β 2. In each panel, protein is shown in cartoon

891 representation, darobactin as sticks (blue = carbons, red = oxygens, white = protons, navy =

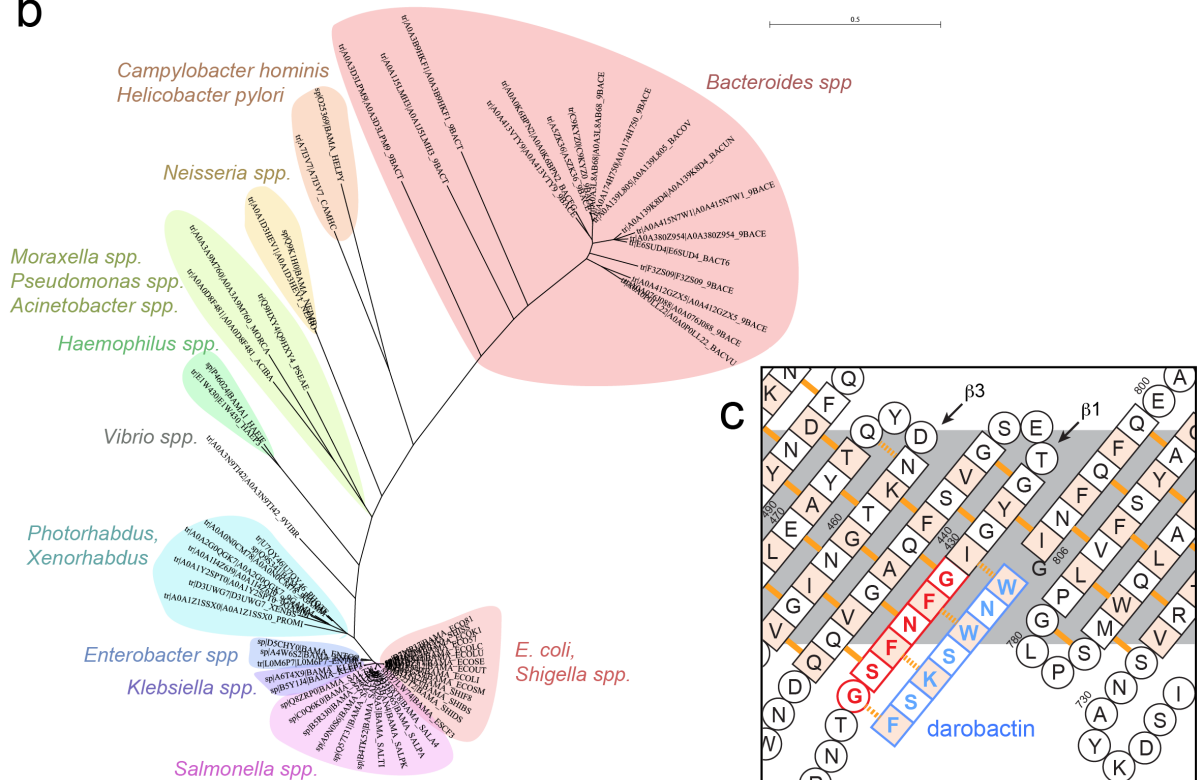
892 nitrogens). Hydrogen bonds are shown as black dotted lines.

a

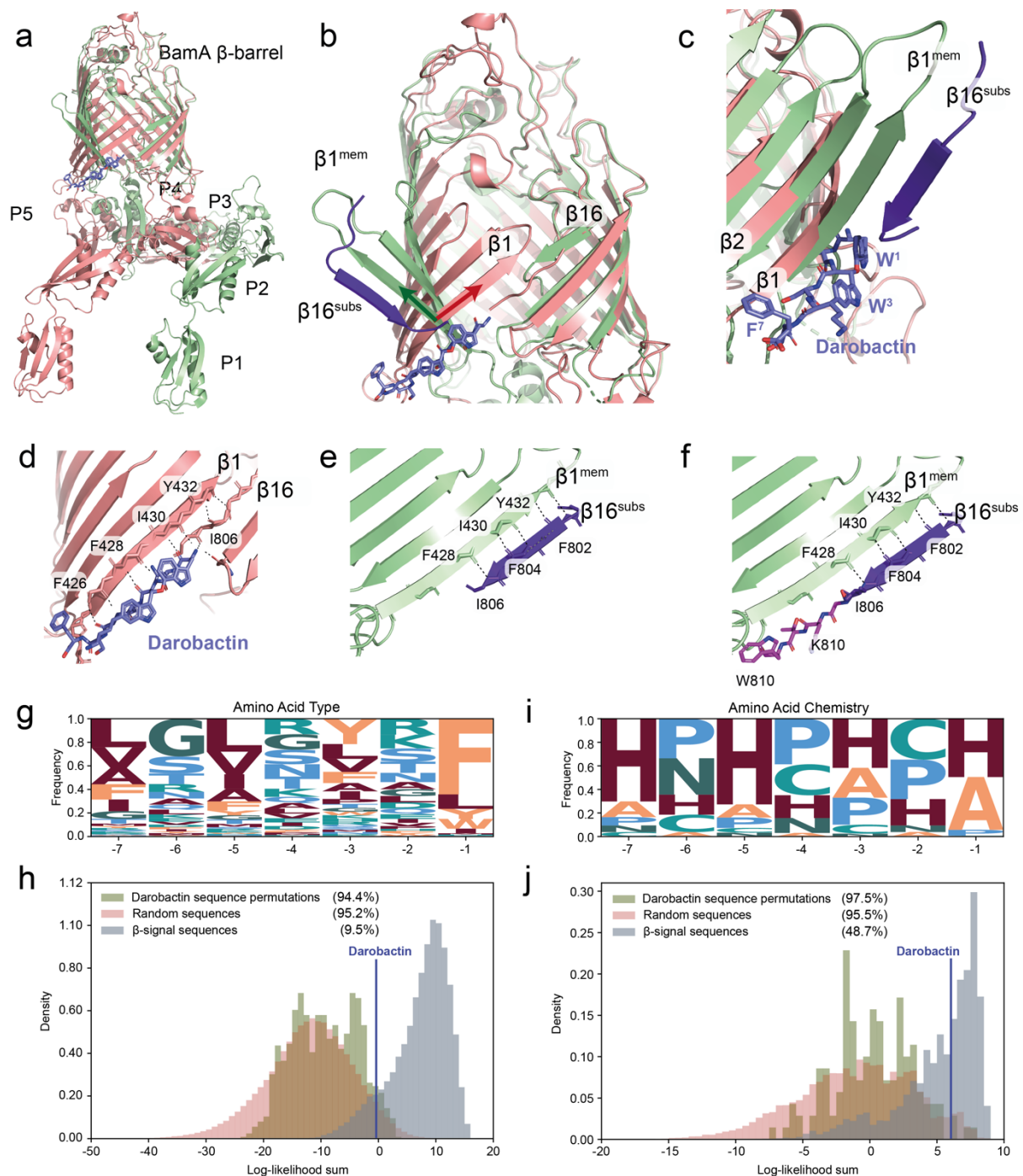
<i>Bacteroides vulgatus</i>	PTNGTVDINWNLESKANDQVEFSAGWGQTVGIG-	471	DQVEFS
<i>Bacteroides dorei</i>	PTNGTVDINWNLESKANDQVEFSAGWGQTVGIG-	471	
<i>Bacteroides fragilis</i>	PVNGTVDIAIDLVSKANDQVEFSSAGWGQTVGIG-	470	
<i>Bacteroides nordii</i>	PMNGTVDIAIDLVS KANDQVEFS SAGWGQTVGIG-	471	
<i>Bacteroides xylanisolvens</i>	PMNGTVDIGLPLTSKANDQVEFSAGWGQTVGIG-	471	
<i>Bacteroides caccae</i>	PMNGTVDIGLPLTSKANDQVEFSAGWGQTVGIG-	471	
<i>Enterobacter cloacae</i>	-SPDQVDVVYVKERNTGSFNFGVGYGTESGVSF	440	GSFNFG
<i>Klebsiella pneumoniae</i>	-SPDQVDVVYVKERNTGSFNFGVGYGTESGVSF	440	
<i>Shigella dysenteriae</i>	-SPDQVDVVYVKERNTGSFNFGVGYGTESGVSF	440	
<i>Shigella sonnei</i>	-SPDQVDVVYVKERNTGSFNFGVGYGTESGVSF	440	
<i>Escherichia coli</i>	-SPDQVDVVYVKERNTGSFNFGVGYGTESGVSF	440	
<i>Salmonella paratyphi</i>	-SPDQVDVVYVKERNTGSFNFGVGYGTESGVSF	440	
<i>Salmonella typhimurium</i>	-SPDQVDVVYVKERNTGSFNFGVGYGTESGVSF	440	
<i>Neisseria gonorrhoeae</i>	-TPDKVDLNM SLTERSTGSLDL SAGWQDTGLVM	440	GXXXXX (GTTTLA)
<i>Haemophilus influenzae</i>	-SNDEVVVYVKERNTGSINFGVGYGTESGISY	437	
<i>Pseudomonas aeruginosa</i>	-TDDQVDVNVSVVEEQPSGSITASVGFQAQAGLIL	439	
<i>Moraxella catarrhalis</i>	-SPDQVDVNFVVEEQPSGSSTIAAGYSQSGGVTF	446	
<i>Acinetobacter baumannii</i>	---SPDQVDLNVNVEEQHSGTTTLAVGYSQSGGITF	444	
<i>Helicobacter pylori</i>	---SLMDLLVSVVEEGRTGQLQFGLGYGSYGGLML	485	
<i>Campylobacter hominis</i>	---DQIDLEVVVKEAPTGSVTGGVGYGSNDGLLL	435	
<i>Proteus mirabilis</i>	-SPDQVDIVYVKERNTGSLNFGVGFGTESGVSF	440	
<i>Photorhabdus luminescens</i>	-SPDQVDVVYVKERNTGSLNFGVGFGTESGVSF	440	
<i>Photorhabdus temperata</i>	-SPDQVDIVYVKERNTGSLNFGVGFGTESGVSF	440	
<i>Xenorhabdus japonica</i>	-SPDQVDVVYVKERNTGSMNFGVGFGTESGMSF	440	
<i>Xenorhabdus hominickii</i>	-SPDQVDVVYVKERNTGSMNFGVGFGTESGMSF	458	

Darobactin interaction site

b



894 **Extended Data Fig. 8. Relatedness of predicted Gram-negative BamA proteins. (a)**
895 Sequence alignment of BamA sequence from Gram-negative bacteria. The region highlighted
896 in yellow is the predicted interaction site of darobactin in sheet β 1. Right hand side: This 6
897 amino acid sequence of *A. baumannii* and *B. fragilis* was substituted into *E. coli* BamA for *in*
898 *vivo* assays. (b) Phylogenetic tree of full length BamA sequences from various species of
899 Gram-negative bacteria. Different colours indicate different branches belonging to the species
900 specified next to the branch. Multiple alignments for the tree were carried out using
901 CLUSTAL-W and the phylogenetic tree was derived using SEAVIEW software. (c) Topology
902 plot of BamA from *E. coli* with bound darobactin (blue). For the chimeric mutants the red
903 amino acids were exchanged with the local sequence from either *A. baumannii* or *B. fragilis*.
904
905



906

907

908 **Extended Data Fig. 9. Comparison of BamA structures involved in molecular interactions**

909 **and analysis of β -signals.** (a) Overlay of the BamA subunit from the BAM–darobactin

910 complex (salmon–blue; this work) with a BamA engaged with a substrate in a late-stage

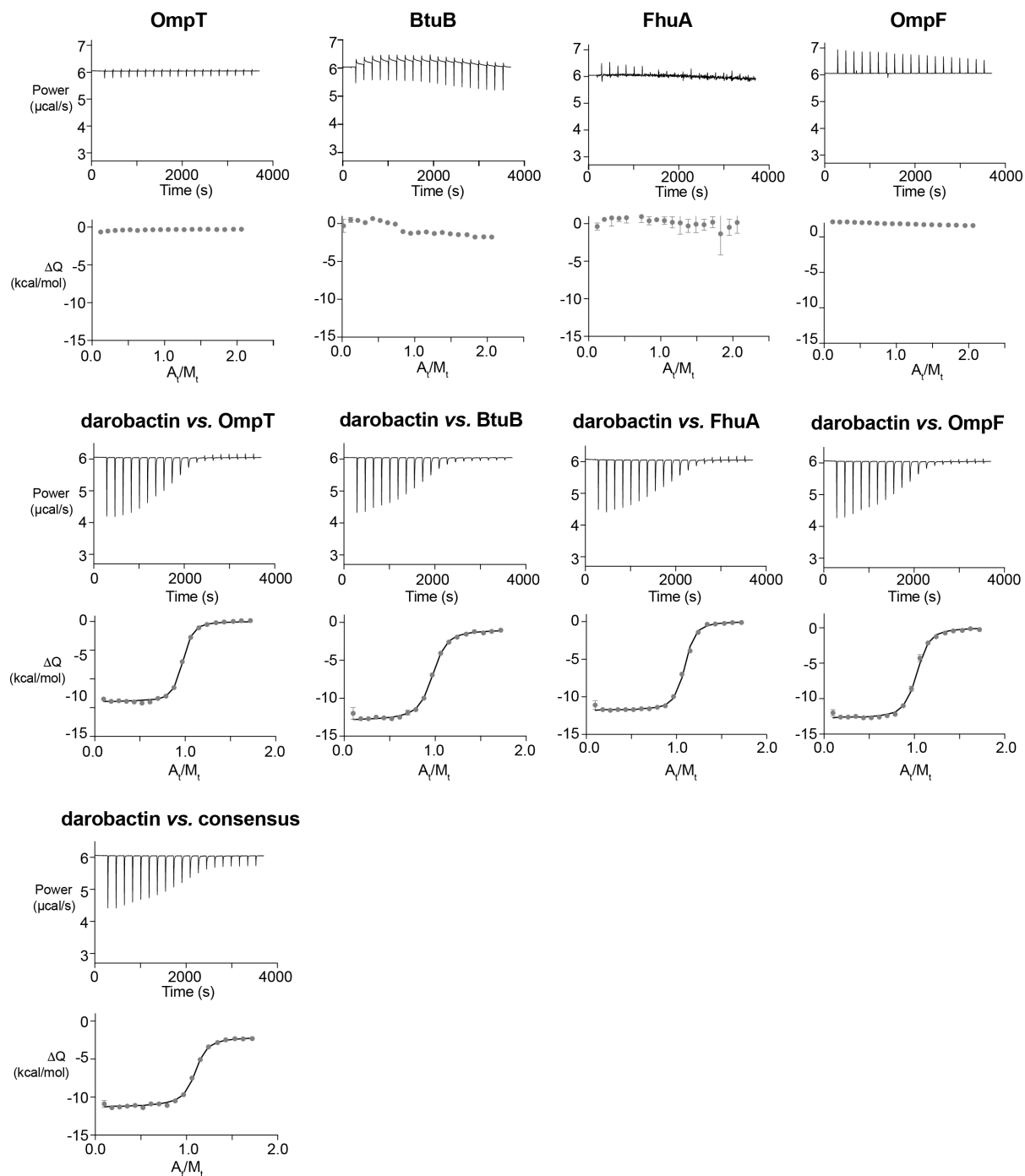
911 insertion intermediate state (green; PDB 6V05). The substrate has been omitted in this panel.

912 The structures have been globally aligned to the protein backbone. (b) Zoom of the same

913 overlay to the BamA b-barrel. Strand $\beta 16^{subs}$ of the substrate is now shown in purple. It is

914 paired to strand $\beta 1^{mem}$ of the catalytic BamA. Bold green and red arrows depict the directions

915 of strand $\beta 1$, forming an $\sim 90^\circ$ angle. (c) Zoom into the gate region indicating the spatial
916 proximity of the substrate and darobactin interaction sites and their relative rotation of $\sim 90^\circ$.
917 (d–f) Comparison of the register of $\beta 16$ complementation to $\beta 1$. (d) In BamA–darobactin
918 (salmon), residue I806 pairs with Y432. (e) In the late stage intermediate, I806 of the substrate
919 BamA^{subs} (purple) pairs with F428 in catalyst BamA^{mem} (green), corresponding to a register
920 shift of 4. (f) Hypothetical position of the four C-terminal residues of substrate BamA, which
921 are not resolved in the available electron density. When paired to $\beta 1^{\text{mem}}$ in canonical
922 antiparallel β -strand conformation, they locate exactly at the darobactin binding site, with the
923 C-terminal W810 at the position of F⁷ of darobactin. (g) Frequency logo of known and putative
924 β -signals from bacterial OMPs, colored by amino acid chemistry. Numbering refers to distance
925 from C-terminus. (h) Distribution of log-likelihood scores in three different sets of sequences,
926 as indicated. The score obtained by the darobactin sequence is indicated by a blue line. The
927 percentile rank of darobactin within each of the three sets is given in brackets. (i,j) Same as g,
928 h, but based on side chain chemistry. “H” = hydrophobic and non-polar residue; “A” =
929 aromatic; “N” = neutral; “C” = charged; “P” = polar non-charged.



930

931 **Extended Data Fig. 10. Interaction of β -signal peptides with BamA- β barrel in detergent**

932 **micelles by isothermal titration calorimetry.** The first 4 panels show a direct titration of each

933 of the 10aa long β -signal peptides of BamA, BtuB, FhuA, and OmpF to the BamA- β barrel.

934 The next 5 panels show a competition experiment of darobactin titrated to BamA- β barrel in

935 the presence of 10aa long β -signal peptides of OmpT (0.7 mM), BtuB (2.6 mM), OmpF (1.4

936 mM), FhuA (1.1 mM) and a β -consensus-peptide (1.2 mM). The results from fitting of the data

937 to the competition model is given in Supplementary Table 7.

938